

# JOURNAL OF UMM AL-QURA UNIVERSITY *for Applied Sciences*



جامعة أم القرى  
UMM AL-QURA UNIVERSITY

 Springer



# Journal of Umm Al-Qura University for Applied Sciences

Publishing model  
**Open access**

[Submit your manuscript](#) →



[Editorial board](#)

[Aims and scope](#)

[Journal updates](#)

## Editors

### EDITOR-IN-CHIEF

**Basim H. Asghar:** Faculty of Science, Umm Al-Qura University, Saudi Arabia  
Email: bhasghar@uqu.edu.sa

### CHIEF EDITOR CHEMISTRY

**Saleh A. Ahmed:** Assiut University, Egypt

### CHIEF EDITOR PHYSICS

**Adel Mohamed Hashmi Madani:** Carthage University, Tunisia

### CHIEF EDITOR BIOLOGY

**Hussein Hasan Abulreesh:** Faculty of Science, Umm Al-Qura University, Saudi Arabia

### CHIEF EDITOR MATHEMATICS

**Rajaa Taher Mohammad Matoog:** Faculty of Science, Umm Al-Qura University, Saudi Arabia

### CHIEF EDITOR EARTH & ENVIRONMENT

**Antonis A. Zorpas:** Pure and Applied Sciences, Open University of Cyprus, Nicosia, Cyprus

### ASSOCIATE EDITORS CHEMISTRY

- Alaa S. Abd-El-Aziz:** University of Prince Edward Island, Canada
- Imran Ali:** Chemistry Department, Jamia Millia Islamia University, New Delhi, India
- Abdulrahman A. Alwarthan:** King Saud University, Riyadh, Saudi Arabia
- Grzegorz Boczkaj:** Gdansk University of Technology, Gdansk, Poland
- Jibran Iqbal:** Zayed University, United Arab Emirates
- Mohammad Mansoob Khan:** Dept of Chemical Sciences, Universiti Brunei Darussalam, Brunei Darussalam
- Tawfik A. Khattab:** National Research Centre, Cairo, Egypt
- Mu. Naushad:** College of Science, King Saud University, Riyadh, Saudi Arabia
- Van-Huy Nguyen:** Institute of Medicinal Technopreneurship and Advanced Training, Vietnam
- Fawaz A. Saad:** Umm Al-Qura University, Saudi Arabia
- Noor Samad Shah:** COMSATS University Islamabad, Vehari Campus, Pakistan
- Essam M. Hussein:** Assiut University, Egypt

### ASSOCIATE EDITORS PHYSICS

- Atif Mossad Ali:** King Khalid University, Saudi Arabia
- Ameer Azam:** Aligarh Muslim University, Aligarh, India
- Mohamed Shaban Said Fadel:** Islamic University of Madinah, Saudi Arabia
- Boon Tong Goh:** University of Malaya, Kuala Lumpur Malaysia
- Alamgir Karim:** University of Houston, USA
- Shaaban Khalil:** Zewail City of Science and Technology, Giza, Egypt
- Abdel-Aleam H. Mohamed:** Taibah University, Saudi Arabia
- Roshdi Seoudi Mohamed:** National Research Centre, Physics Research Institute, Egypt
- Abderrahim Wakif:** Hassan II University of Casablanca, Morocco

### ASSOCIATE EDITORS BIOLOGY

- Mohamed Hashem:** King Khalid University, Saudi Arabia
- Muhammad Amjad Bashir:** Ghazi University, Pakistan
- Abdelhamid Elaissari:** University Claude Bernard Lyon-1, Lyon, France
- Mohamed Fawzy Ramadan:** Faculty of Applied Medical Sciences, Umm Al-Qura University, Saudi Arabia
- Hayat Shamsul:** Aligarh Muslim University, Aligarh, India
- Hifzur R. Siddique:** Department of Zoology, Aligarh Muslim University, India
- Iqbal Ahmad:** Aligarh Muslim University, INDIA

### ASSOCIATE EDITORS MATHEMATICS

- M. Ali Akbar:** Rajshahi University, Bangladesh
- Isaac Lare Animasau:** Federal University of Technology Akure, Nigeria
- Omar Abu Arqub:** Al Balqa Applied University, Jordan
- Dumitru Baleanu:** Cankaya University, Turkey
- Muhammad Mubashir Bhatti:** Shandong University of Science and Technology, China
- José Francisco Gómez Aguilar:** Conahcyt/Tecnm-Cenidet University, Cuernavaca Morelos, México
- Wen-Xiu Ma:** University of South Florida, USA
- Mohamed S. Osman:** Faculty of Science, Cairo University, Egypt
- Youssri Hassan Youssri:** Cairo University, Egypt

### ASSOCIATE EDITORS EARTH & ENVIRONMENT

- Sudip Chakraborty:** Department of DIMES, University of Calabria, Italy
- Shah Fahad:** Abdul Wali Khan University, Pakistan
- Riheb Hadji:** University of Setif 1, Setif, Algeria
- Younes Hamed:** University of Gafsa, Tunisia
- Muhammad Zaffar Hashmi:** University of Lahore, Pakistan
- Bassem Sayed Nabawy:** National Research Center, Cairo, Egypt

### MANAGING EDITOR

**Nahla A. Tayyib**  
Deanship of Scientific Research, Umm Al-Qura University, Saudi Arabia  
Email: natayyib@uqu.edu.sa

## For authors

- [Submission guidelines](#) →
- [Language editing services](#) →
- [Ethics and disclosures](#) →
- [How to publish with us](#) →
- [Contact the journal](#) →
- [Collections and calls for papers](#) →



**Language quality checker**  
[Get your manuscript edited for free](#) →

[Use our pre-submission checklist](#) →  
Avoid common mistakes on your manuscript.

[This journal's calls for papers](#) →  
Collections this journal is participating in.

[Sign up for alerts](#) →  
Get notified when new articles are published.

## Explore

- [Articles](#) →
- [Volumes and issues](#) →
- [Collections](#) →

## Discover content

- [Journals A-Z](#)
- [Books A-Z](#)

## Publish with us

- [Publish your research](#)
- [Open access publishing](#)

## Products and services

- [Our products](#)
- [Librarians](#)
- [Societies](#)
- [Partners and advertisers](#)

## Our imprints

- [Springer](#)
- [Nature Portfolio](#)
- [BMC](#)
- [Palgrave Macmillan](#)
- [Apress](#)



## Articles

Search all Journal of Umm Al-Qura University for Applied Sciences articles →

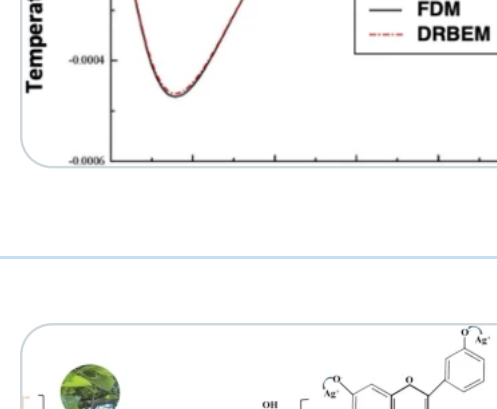
Filter by	Sort by
Volume: <input type="text" value="All volumes"/>	Date published: <input checked="" type="radio"/> New to old <input type="radio"/> Old to new
<b>Update results</b> ↻	

Showing 1–50 of 181 articles

### Separation axioms on fuzzy neutrosophic bitopological spaces using fuzzy neutrosophic open sets

 Saikh Shahjahan Miah, Farhata Tabassum Lily ... M. Ali Akbar  
 Original Article | Open access | 12 August 2024

### Removal of antibiotics from wastewater using nanoparticles-based technology: a review

 Muhammad Zaffar Hashmi, Afraz Habib & Ahmad Hasnain  
 Review | Open access | 10 August 2024


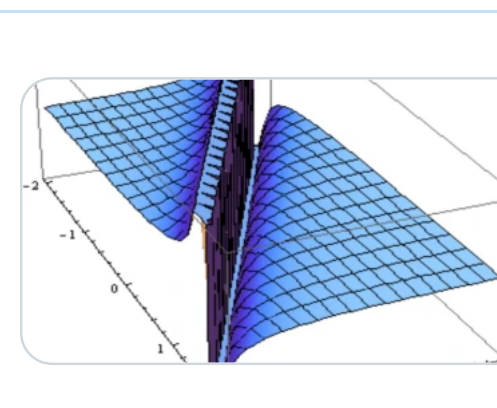
### A time-stepping DRBEM for nonlinear fractional sub-diffusion bio-heat ultrasonic wave propagation problems during electromagnetic radiation

 Mohamed Abdelabour Fahmy  
 Original Article | Open access | 08 August 2024

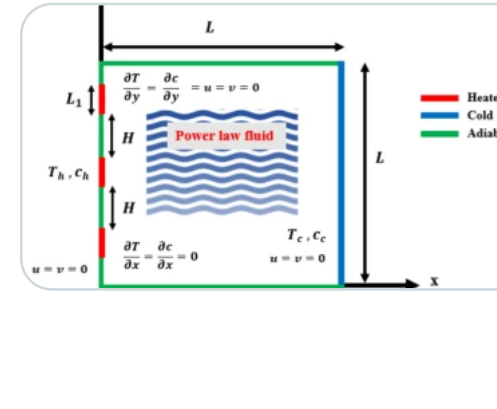

### Synthesis of Silver and Copper oxide nanoparticles using Ficus racemosa leaf extract: characterization, anticancer potential, and dye degradation efficacy

 Akhilesh Kumar Maurya, Shagun Varshney ... Nidhi Mishra  
 Original Article | Open access | 27 July 2024


### The contribution of microorganisms to sustainable development: towards a green future through synthetic biology and systems biology

 Alaa T. Qumsani  
 Review | Open access | 26 July 2024


### Gradient discretisation of elliptic quasi-variational inequalities with gradient type barriers

 Yahya Alnashri  
 Original Article | Open access | 24 July 2024


### Modified simple equation technique for first-extended fifth-order nonlinear equation, medium equal width equation and Cauchy–Dodd–Gibson equation

 A. K. M. Kazi Sazzad Hossain, M. Ali Akbar & Md. Ismail Hossain  
 Original Article | Open access | 18 July 2024


### Implementing the finite element numerical approach to optimize thermosolutal convection (TSC) energy imparted by discrete heat and solute sources in generalized Newtonian fluid flow in square enclosure

 S. Bilal, Haider Ali ... Dumitru Baleanu  
 Original Article | Open access | 16 July 2024


### Securing a sustainable future: the climate change threat to agriculture, food security, and sustainable development goals

 Anam Saleem, Sobia Anwar ... Touqir Nawaz  
 Review | Open access | 11 July 2024

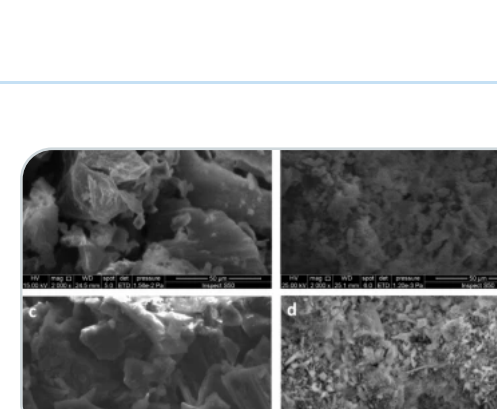

### Comprehensive modeling and simulation of photovoltaic system performance by using matlab/simulink: integrating dynamic meteorological parameters for enhanced accuracy

 Mohamed Nfaoui, Fatima Ezzahra Ibra ... Khalil El-Hami  
 Original Article | Open access | 05 July 2024

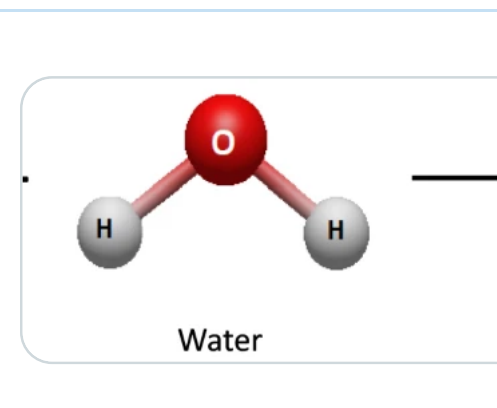

### Exogenous application of citric acid mitigates salt-induced oxidative stress in Moringa oleifera seedlings

 Aref Nasraoui Hajaji, Houda Maaroufi-Dguimi & Youssef Ammari  
 Original Article | Open access | 05 July 2024


### Extending the shelf-life of refrigerated chicken fillets by using polymeric coating layer composed of ginger Zingiber officinale essential oil loaded-chitosan nanoparticles

 Safa Musalem, Mounir Mahmoud Hamdy ... Nermeen Makram Louis Malak  
 Original Article | Open access | 01 July 2024


### Adsorption of Red 141 and methylene blue by cuttlebone: experimental and molecular dynamics study

 Abdellatif Aarfane, Meryem Bensemlali ... Hamid Nasreallah  
 Original Article | Open access | 28 June 2024


### Sample size calculation in biomedical, clinical and biological sciences research

 Idris Zubairu Sadiq, Abubakar Usman ... Kabiru Halliru Ahmad  
 Review | Open access | 26 June 2024

### Organotin complexes with Schiff's base ligands: insights into their cytotoxic effects on lung cancer cells

 Falih Ibadi, Emad Yousif ... Nany Hairunisa  
 Original Article | Open access | 25 June 2024


### Exploring ocean pH dynamics via a mathematical modeling with the Caputo fractional derivative

 Manisha Krishna Naik, Chandrali Baishya ... P. Veerasha  
 Review | Open access | 24 June 2024

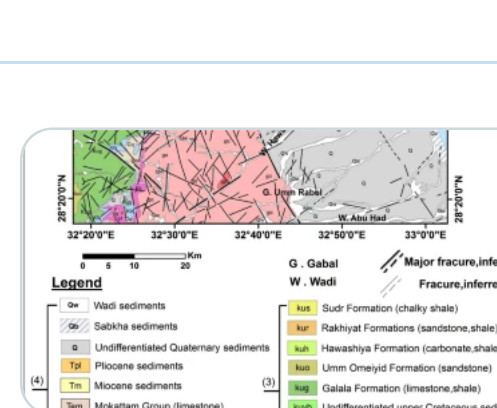

### Synthesis of silver nanoparticles as an antimicrobial mediator

 Khadija Khalidoun, Sumera Khizar ... Abdelhamid Elaissari  
 Review | Open access | 21 June 2024

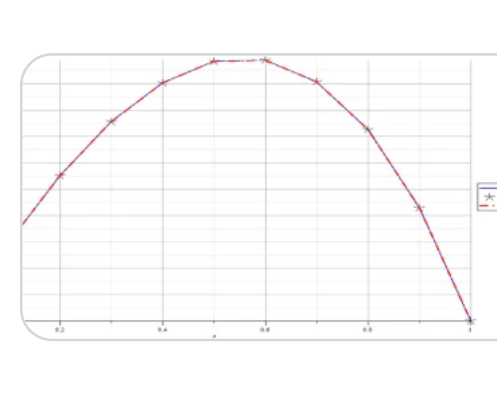

### Spectrophotometric determination of cobalt ions in water using bimetallic chemosensor based on sulfa drug azo dye

 Sulafa Nassar & Gharam I. Mohammed  
 Original Article | Open access | 04 June 2024

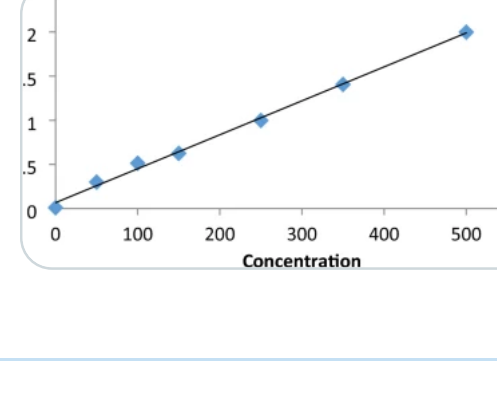

### Screening and evaluation of antibacterial active strains of Actinomycetes isolated from Northern Indian soil for biofilm inhibition against selected ESKAPE pathogens

 Muzammil Sharief Dar & Iqbal Ahmad  
 Original Article | Open access | 04 June 2024


### Physical methods for preparation of nanomaterials, their characterization and applications: a review

 Nuha Al-Harbi & Nabil K. Abd-Elahman  
 Review | Open access | 30 May 2024


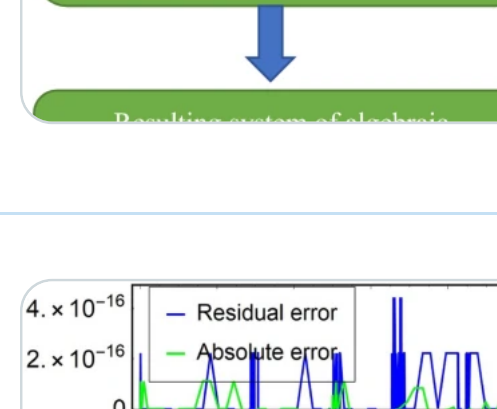
### Helicobacter pylori infection in Africa: comprehensive insight into its pathogenesis, management, and future perspectives

 Blessing N. Emmanuel, Deborah A. Peter ... Kayode Olafifa  
 Review | Open access | 30 May 2024


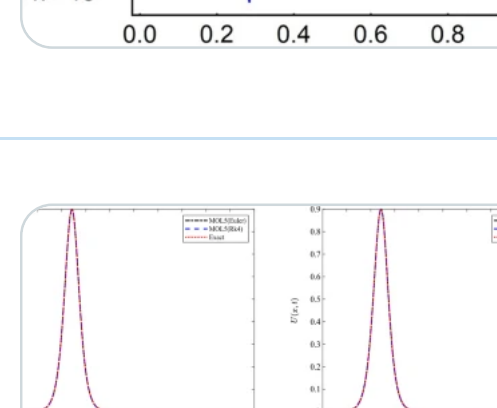
### On Grüss, Ostrowski and trapezoid-type inequalities via nabla integral on time scales

 Ammara Nosheen, Khuram Ali Khan & Iram Shahzadi  
 Original Article | Open access | 24 May 2024

### Delineating the uranium anomalous zones using remote sensing and radiometric data: a case study from Gabal Umm Tinassib area, North Eastern Desert, Egypt

 Assran Sayed Mohamed Assran, Reda Abu Yousef El Qassas ... Manal Mohamed Othman  
 Original Article | Open access | 23 May 2024


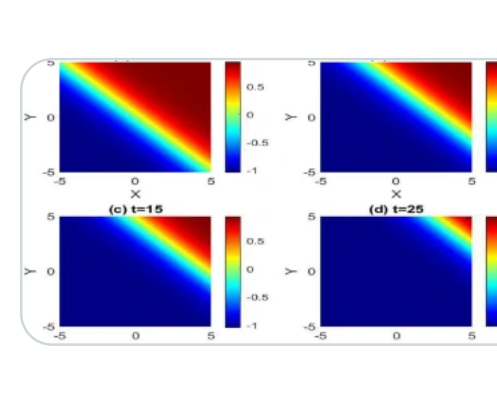
### Efficient decomposition shooting method for tackling two-point boundary value models

 H. O. Bakodah, Kholoud A. Alzahrani ... Mariam H. Almazmumy  
 Original Article | Open access | 22 May 2024


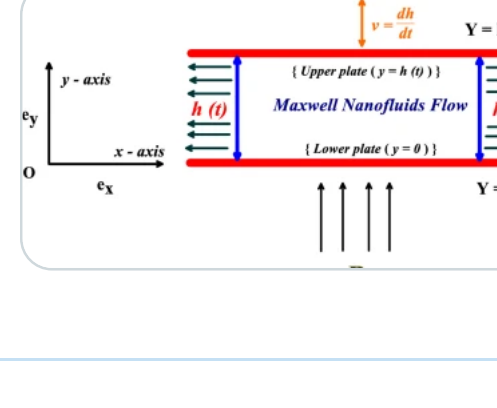
### Biological activity, chemical composition, and molecular docking of Eugenia punicifolia (Kunth) DC

 Abdurahman Mahmoud Dogara, Muhammad Tukur Ibrahim ... Kamal Tabti  
 Original Article | Open access | 16 May 2024


### Green and sustainable synthesis of the ZnONPs using leaf extract of Guazuma ulmifolia for antioxidant and antimicrobial activities

 Salah Eldeen Dafalla, Nayef Abdulaziz Aldabaan ... Veeranna S. Hombalimath  
 Original Article | Open access | 16 May 2024


### Numerical approximation of the typhoid disease model via Genocchi wavelet collocation method

 G. Manohara & S. Kumbinarasalah  
 Original Article | Open access | 09 May 2024


### The improved residual power series method for the solutions of higher-order linear and nonlinear boundary value problems

 Rimshah Gillani, Abdullah Dawar & Hamid Khan  
 Original Article | Open access | 04 May 2024

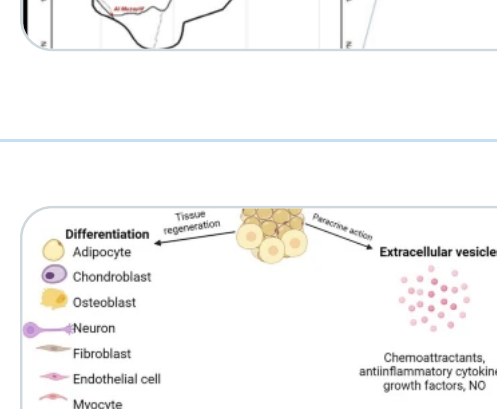

### Non-central m-point formula in method of lines for solving the Korteweg-de Vries (KdV) equation

 A. Alshareef & H. O. Bakodah  
 Original Article | Open access | 03 May 2024


### Environmental challenges and air pollution in Bac Lieu, Vietnam: assessing sources and impacts

 Ton That Lang, Tran Quoc Thao ... Nguyen Nhat Huy  
 Original Article | Open access | 03 May 2024

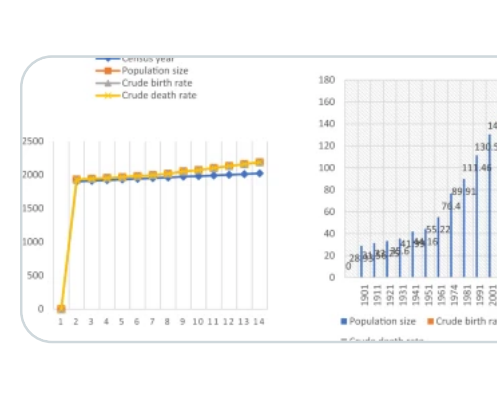

### Exact solutions for travelling waves using Tanh method for two dimensional stochastic Allen–Cahn equation with multiplicative noise

 Hasan Alzubaidi  
 Original Article | Open access | 02 May 2024


### New insights into MHD squeezing flows of reacting–radiating Maxwell nanofluids via Wakif's–Buongiorno point of view

 Amine El Harfouf, Abderrahim Wakif & Sanaa Hayani Mounir  
 Original Article | Open access | 30 April 2024


### Availability and saccharification of starchy biowastes for bioethanol production in the Kingdom of Saudi Arabia

 Fadha Al-Malki, Saad Alamri & Mohamed Hashem  
 Original Article | Open access | 30 April 2024


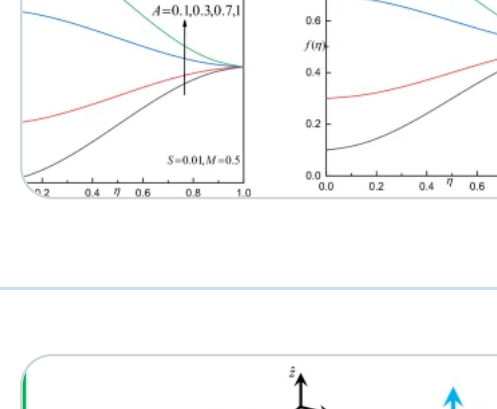
### Haque's approach with mickens' iteration method to find a modified analytical solution of nonlinear jerk oscillator containing displacement time velocity and time acceleration

 Md. Ishaque Ali, B. M. Ikramul Haque & M. M. Ayub Hossain  
 Original Article | Open access | 30 April 2024

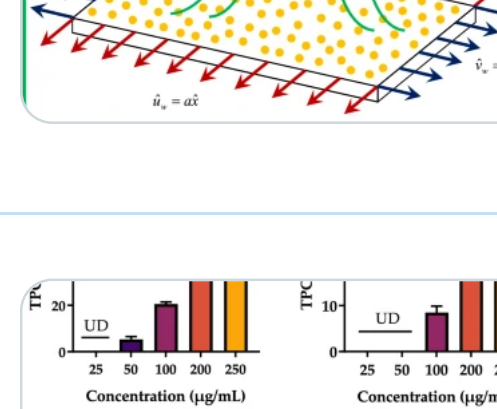

### Mathematical analysis of a within-host dengue virus dynamics model with adaptive immunity using Caputo fractional-order derivatives

 Morufu Oyedunsi Olayiwola & Akeem Olarewaju Yunus  
 Original Article | Open access | 26 April 2024

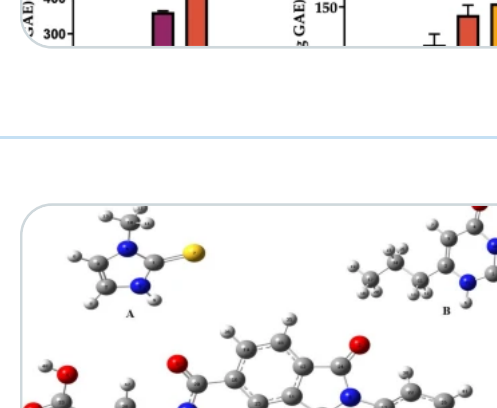

### Prevalence of tick infestation and molecular characterization of tick species of camels (Camelus dromedarius) from Al-Baha South Saudi Arabia

 Samia Q. Alghamdi  
 Original Article | Open access | 26 April 2024


### Current progress and limitations of research regarding the therapeutic use of adipose-derived stem cells: literature review

 Maksym Skrypyuk  
 Review | Open access | 17 April 2024


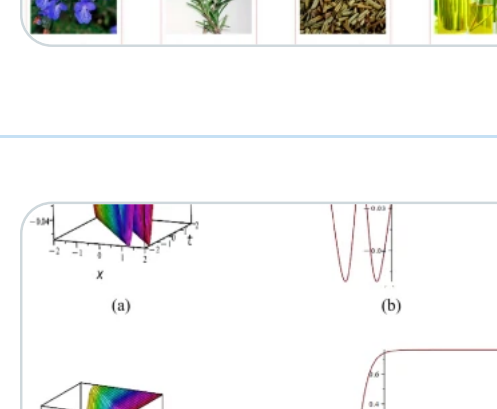
### Green extraction of anthocyanins from Syzygium cumini fruit pulp using aqueous glycerol through ultrasound-assisted extraction

 Darshanjot Kaur & Ovais Shafiq Qadri  
 Original Article | Open access | 17 April 2024


### A study about the prediction of population growth and demographic transition in Bangladesh

 Rezaul Karim, M. A. Bkar Pk ... M. S. Osman  
 Original Article | Open access | 15 April 2024


### Evaluation of bacteriostatic and antioxidant activities of various extracts from aerial part of Piper nigrum grown in Gulf countries traditionally used for the treatment of various infectious diseases

 Doaa Ibrahim Marey Alateeqi, Salem Said Jarouf Al-Touby & Mohammad Amzad Hossain  
 Original Article | Open access | 13 April 2024


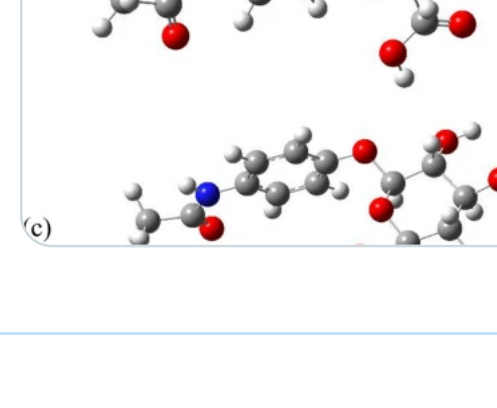
### Comparative and interactive response of salicylic acid, 2,4-epibrassinolide or sodium nitroprusside against cadmium stress in Linum usitatissimum

 Sabreena Nazir, Yamshi Arif ... Hayat Shamsul  
 Original Article | Open access | 12 April 2024


### Cross diffusion effects on MHD double diffusive viscous flow through Hermite wavelet method

 Suma Nagendrapa Nagappanavar, K. R. Raghunatha & D. L. Kiran Kumar  
 Original Article | Open access | 11 April 2024


### Further insights into steady three-dimensional MHD Sakiadis flows of radiating-recting viscoelastic nanofluids via Wakif's–Buongiorno and Maxwell's models

 Abderrahim Wakif, Mostafa Zaydan & Rachid Sehaoui  
 Original Article | Open access | 09 April 2024


### Glycemic homeostasis of ultrasound-assisted Murraya koenigii (Linn.) Spreng. bark extract in streptozocin-induced diabetes in rats

 Naiyer Shahzad  
 Original Article | Open access | 06 April 2024


### DFT studies on structure, electronics, bonding nature, NBO analysis, thermodynamic properties, molecular docking, and MM-GBSA evaluation of 4-methyl-3-[2-(4-nitrophenyl)-1,3-dioxo-2,3-dihydro-1H-isoindole-5-amido]benzoic acid: a potent inhibitor of Graves' disease

 Emmanuel Israel Edache, Adamu Uzairu ... Muhammad Tukur Ibrahim  
 Original Article | Open access | 05 April 2024


### Rosmarinus officinalis Linn.: unveiling its multifaceted nature in nutrition, diverse applications, and advanced extraction methods

 Hanee Meziane, Linda Zraïbi ... Rachid Touzani  
 Review | Open access | 03 April 2024


### Soliton solutions to a nonlinear wave equation via modern methods

 Shuvo Sarker, Rezaul Karim ... Pinakee Dey  
 Review | Open access | 27 March 2024


### A comprehensive review on phytochemicals as potential therapeutic agents for stress-induced gastric ulcer

 Naiyer Shahzad, Ibrahim Abdel Aziz Ibrahim ... Mohd Fahami Nur Azlina  
 Review | Open access | 27 March 2024


### The early Danian event (Dan-C2) and the latest Danian event (LDE): a case study from Gebel Kilabiya, Egypt

 Orabi H. Orabi, Heba Ismail & Saïda Taha  
 Review | Open access | 25 March 2024


### Thermodynamics analysis of acetaminophen and its metabolites using density functional theory

 Abdel-baset H. Mekky  
 Original Article | Open access | 20 March 2024




# Organotin complexes with Schiff's base ligands: insights into their cytotoxic effects on lung cancer cells

Falih Ibad<sup>1</sup> · Emad Yousif<sup>1</sup> · Ahmed Al-Ani<sup>1</sup> · Mohammed. Al-Mashhadani<sup>1</sup> · Ali Z. Al-Saffar<sup>2</sup> · Ali Basem<sup>3</sup> · Muna Bufaroosha<sup>4</sup> · Hassan Hashim<sup>5</sup> · Amani Husain<sup>6</sup> · Ali H. Jawad<sup>7</sup> · Nany Hairunisa<sup>8</sup>

Received: 24 April 2024 / Accepted: 18 June 2024  
© The Author(s) 2024

## Abstract

Organotin(IV) complexes can be used in chemotherapy due to its lipophilicity which can be affected by the availability of Sn coordination bond and bond stabilization between ligand and Sn(IV). In this study, three types of tri-organotin(IV) complexes which are, Ph<sub>3</sub>SnL, Me<sub>3</sub>SnL, and Bu<sub>3</sub>SnL derived from Schiff base ligand were synthesized by the reaction of methyl dopa with p-dimethylaminobenzaldehyde. All prepared complexes were characterized using nuclear magnetic resonance (<sup>1</sup>H NMR, <sup>13</sup>C NMR, and <sup>119</sup>Sn NMR). The results confirm the coordination of the organotin(IV) moieties to the ligand. The cytotoxicity of tri-organotin(IV) complexes was evaluated against the A549 human lung cancer cell using MTT assay. Ph<sub>3</sub>SnL showed a high cytotoxic effect among other complexes, Bu<sub>3</sub>SnL also showed a significant cytotoxic effect, while Me<sub>3</sub>SnL demonstrated a relatively lower effects. These findings highlight the potential of the tri-organotin(IV) complexes, particularly Ph<sub>3</sub>SnL and Bu<sub>3</sub>SnL, as promising candidates for further modification as anticancer agents. The results obtained from this study can be used to understand the structure–activity of organotin(IV) complexes and their applications as anti-cancer activity.

**Keywords** Tri-organotin(IV) complexes · Anti-drugs cancer · MTT assay · A549 human cell · Half-maximal inhibitory concentration (IC50)

✉ Emad Yousif  
emad\_yousif@hotmail.com

<sup>1</sup> Department of Chemistry, College of Science, Al-Nahrain University, Baghdad, Iraq

<sup>2</sup> Department of Molecular and Medical Biotechnology, College of Biotechnology, Al-Nahrain University, Baghdad, Iraq

<sup>3</sup> Air Conditioning Engineering Department, Faculty of Engineering, Warith Al-Anbiyaa University, Karbala 56001, Iraq

<sup>4</sup> Department of Chemistry, College of Science, UAE University, Al-Ain, UAE

<sup>5</sup> Department of Physics, College of Science, Al-Nahrain University, Baghdad, Iraq

<sup>6</sup> Polymer Research Unit, College of Science, Mustansiriyah University, Baghdad, Iraq

<sup>7</sup> Faculty of Applied Sciences, Universiti Teknologi MARA, 40450 Shah Alam, Selangor, Malaysia

<sup>8</sup> Department of Occupational Medicine, Faculty of Medicine, Universitas Trisakti, Jakarta, Indonesia

## 1 Introduction

Lung cancer is one of the most lethal malignancies, and it remains a significant health challenge in the world. Therefore the demand to continuously improve the therapeutic agents against cancers still is needed [1, 2]. The organotin(IV) complexes have attracted great attention due to their chemical structures and biological activities [3, 4], and they show a potential cytotoxic effect against a number of cancer cell lines [5]. In addition, Schiff base ligands have demonstrated a significant ability in the synthesis of different metal complexes [6–8]. These ligands possess versatile coordination abilities and have been utilized in the preparation of organotin(IV) complexes [9]. Many studies have reported the synthesis and characterization of organotin complexes using Schiff base ligands derived from different aldehydes and amines, and evaluated their activity as anticancer drugs [10]. The biological activity is affected by organic groups and the coordination geometry around the tin atom [11, 12]. The functional groups of the selected ligand can modulate the physicochemical properties of the prepared complexes,

which enhance the anti-cancer activity [13]. Therefore, the synthesized organotin(IV) complexes of new Schiff base ligands considered a good candidate for developing of novel anticancer agents. In terms of cytotoxicity evaluation, the MTT (3-(4,5-dimethyl-2-thiazolyl)-2,5-diphenyl-2H-tetrazolium bromide) colorimetric assay is a widely used to assess cell viability and proliferation [14, 15]. This assay depends on the reduction of MTT by mitochondrial enzymes to formazan crystals, which can be measured by spectrophotometer. By measuring the reduction in cell viability caused by the complexes, the cytotoxic effects and its efficacy against cancer cells can be determined. Several studies have been done to study the cytotoxic properties of organotin(IV) complexes against various cancer cell lines [16, 17]. For example, a research done by Abbas et al. (2022) reported the synthesis of novel organotin(IV) complexes with Schiff base ligands and evaluated their cytotoxicity in vitro in silico bio-activities [18]. The results demonstrated a cytotoxic effects and emphasized the potential of these complexes as anti-cancer agents. Moreover, Wang et al. (2022) prepared a different of organotin(IV) complexes with Schiff base ligands and tested their cytotoxic activities against human lung cancer cells [19]. The complexes exhibited a significant cytotoxicity, demonstrating their potential as anti-lung cancer. Based on the studies done before, organotin(IV) complexes derived from Schiff base ligands considered one of the most important drug to be used as anticancer agent [20, 21]. However, further study needed to explain the structure–activity and optimize the design of these complexes to enhance its efficacy in this field. In this study, we synthesized and characterized different organotin(IV) complexes structures derived from Schiff base compounds to assessed its activity against lung carcinoma epithelial cells (A549 cell line).

## 2 Experimental part

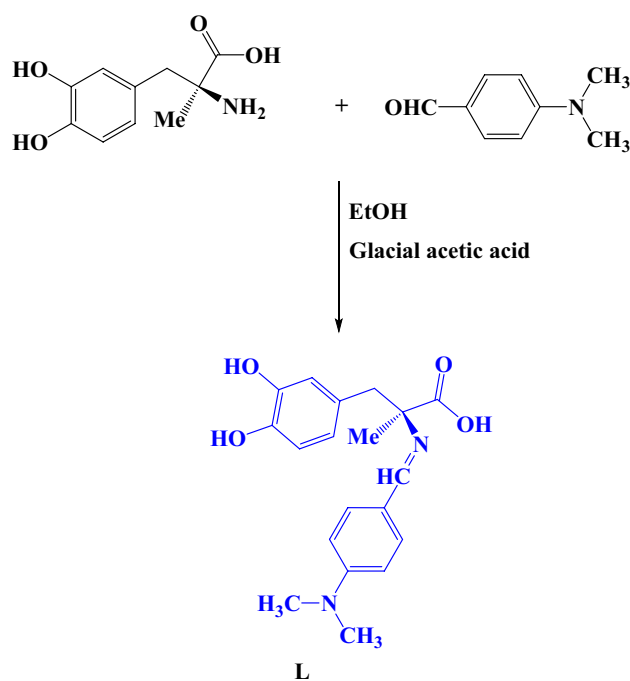
### 2.1 Chemicals

Methyl dopa was purchased from Scharlau Company, while ethanol, methanol, glacial acetic acid, organotin compounds and para-dimethylaminobenzaldehyde were obtained from Fluka.

### 2.2 Characterization

#### 2.2.1 Fourier transform infrared spectroscopy (FTIR)

FTIR spectrometer equipped with an attenuated total reflectance (ATR) accessory (ALPHA II Compact FTIR Spectrometer Bruker) was used in the range (4000–400  $\text{cm}^{-1}$ ) to provide information about functional groups and molecular



**Scheme 1** Synthesis of Schiff base ligand (L)

structure by analyze the absorption bands and transmission of infrared light.

#### 2.2.2 Nuclear magnetic resonance (NMR)

NMR spectroscopy (Bruker) was used to provides information about the chemical structure and connectivity of atoms.

#### 2.2.3 Scanning electron microscopy (SEM)

SEM quanta 450 (FEI, USA) was utilized to get image of the surface morphology and microstructure of samples.

#### 2.2.4 Energy-dispersive X-ray spectroscopy (EDX)

EDS is an elemental analysis to identify the compositions of different elements in a specific sample that combines SEM with X-ray spectroscopy.

### 2.3 Synthesis of Schiff base ligand (L) [22]

A Schiff base was prepared by dissolving 0.25 g (0.1 mol) of methyl dopa and 0.164 g (0.1 mol) of para-dimethylaminobenzaldehyde in 15 mL of ethanol. The mixture was stirred until full dissolve. To catalyzed the reaction, 3 drops of glacial acetic acid were added, and the mixture was refluxed for 3 h as shown in Scheme 1. During this period, a yellow-white precipitate of Schiff base ligand (L) was formed. Then the reaction mixture was cool down to room temperature and

filtrate to get the crude product as yellow-white powder. The crude product was recrystallized twice from ethanol to produce pure target product which was used for further characterization and applications.

## 2.4 Reaction of Schiff base ligand (L) and organotin(IV) complexes

A 0.20 g of synthesized Schiff base ligand was reacted with  $\text{Ph}_3\text{SnCl}$  (0.22 g),  $\text{Bu}_3\text{SnCl}$  (0.20 g), and  $\text{Me}_3\text{SnCl}$  (0.11 g) using 1:1 metal/ligand. The mixtures were refluxed for 6 h at 65 °C in 15 ml methanol as shown in Fig. 2 [23]. The final solutions were filtered, then washing, drying, and recrystallization, to produce  $\text{Ph}_3\text{SnL}$ ,  $\text{Bu}_3\text{SnL}$ , and  $\text{Me}_3\text{SnL}$  complexes as off-white powders (Scheme 2). The physical properties of ligand and synthesized organotin complexes are listed in Table 1.

## 2.5 Cell cultures study

Lung Carcinoma Cells (A549 cell line) was cultured in RPMI-1640 medium with HEPES supplemented with 10% fetal bovine serum (FBS) and 1% penicillin–streptomycin antibiotic and incubated at 37°C in  $\text{CO}_2$  (5%) incubator [24]. When cells reached 80–90% confluency, cells were subcultured into new cell culture dishes using the new RPMI-1640 medium (every 2–3 days). The cell line was provided by the Biotechnology Research Center/Al-Nahrain University.

## 2.6 In vitro cytotoxicity

The cytotoxic potentials of synthesized tri-organotin (IV) complexes were assessed using MTT assay against A549 cells. An aliquot of 200  $\mu\text{L}$  of A549 cells was maintained in 96-well bottom-flat culture plate at a density of  $1 \times 10^5$

**Table 1** The synthesized organotin complexes' physical characteristics

Compounds	Color	Melting point °C	Yield %
L	White	266–268	81
$\text{Ph}_3\text{SnL}$	Off white	290–292	84
$\text{Me}_3\text{SnL}$	Off white	294–296	82
$\text{Bu}_3\text{SnL}$	Off white	297–299	80

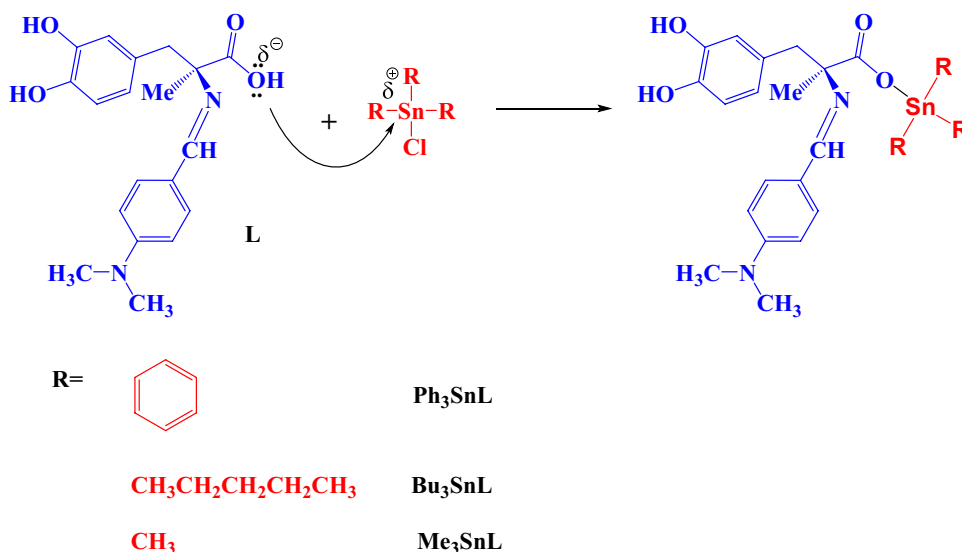
cells/mL. Cells were incubated for 24 h to allow the cells to attach and reach the log phase at the time of tri-organotin (IV) complexes exposure. After incubation, cells were treated with a concentrations of (8, 16, 32, 64, 125, 250, 500 and 1000  $\mu\text{g}/\text{mL}$ ) of the synthesized complexes for 24 h. After incubation, the medium was removed, and cells were labeled with 50  $\mu\text{L}$  of MTT solution (5 mg/mL in phosphate buffer saline) for 4 h at 37°C. The resulting formazan was solubilized with 100  $\mu\text{L}$  dimethyl sulfoxide. Incubation was continued for further 10 min and absorbance was measured at 570 nm using a microtiter plate reader (Bio-Rad, USA). The viability of A549 cells was expressed as a percentage of the value for control value according to the below equation and  $\text{IC}_{50}$  was calculated for each complex depending on viability data [25].

$$\text{Cell Viability (\%)} = \frac{\text{Sample A570}}{\text{Control A570}} \times 100\%$$

## 2.7 Statistical analysis

Statistical analysis was performed using GraphPad Prism version 9.2 (GraphPad Software Inc., La Jolla, CA) to estimate the effect of variable factors on the main study [26]. One-way ANOVA (Tukey Test) was used to determine whether group variance was significant or not. Data were

**Scheme 2** Synthesis of the tri-organotin complexes with proposed mechanism



expressed as mean  $\pm$  standard deviation and statistical difference was considered at the level of  $p < 0.05$ .

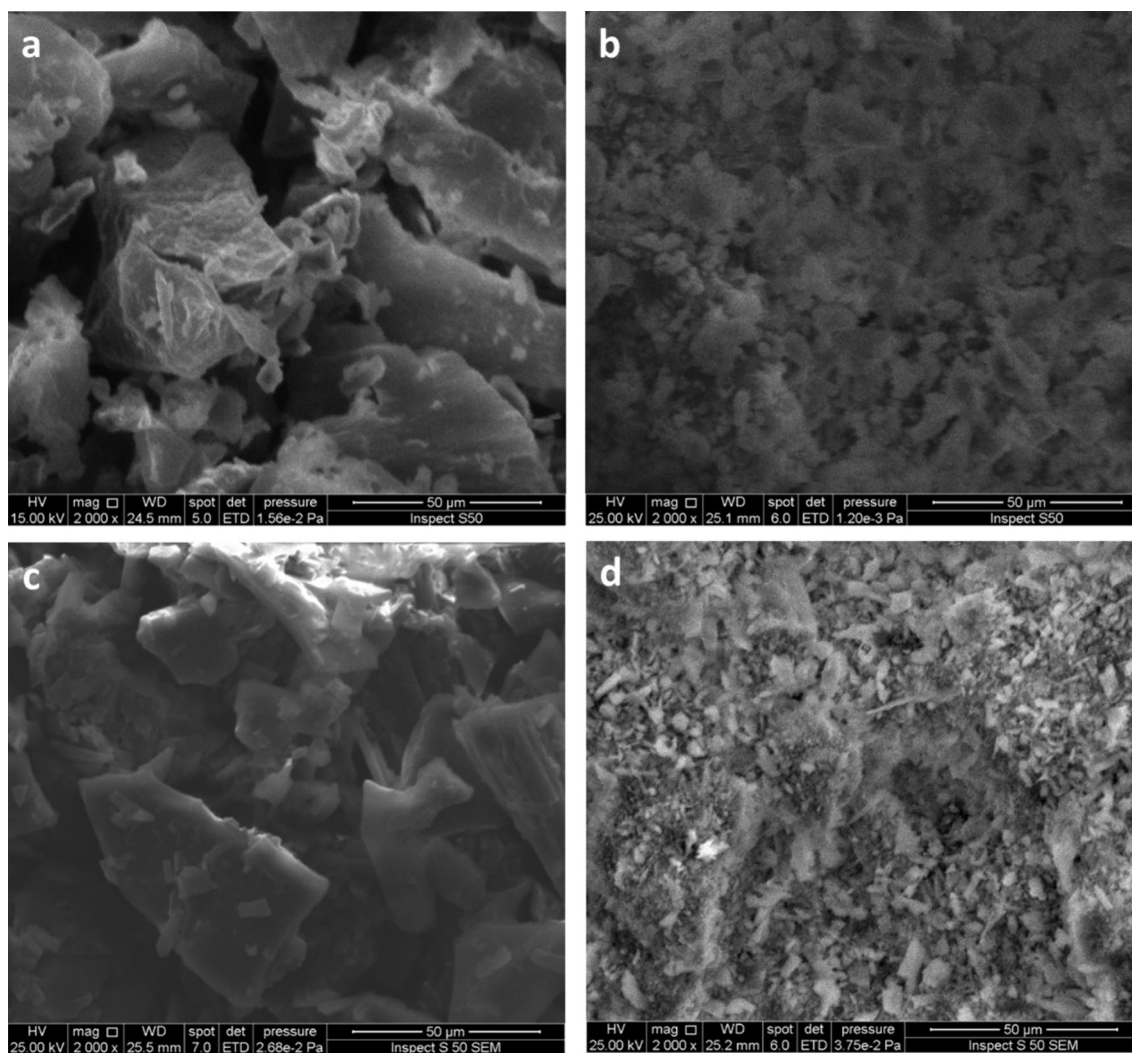
## 2.8 Characterization of synthesized organotin(IV) complexes

### 2.8.1 Scanning electron microscopy (SEM)

SEM was utilized to provides a valuable information about the surface morphology and surface structures of synthesised complexes [27]. Sample prepared by mounted a small amount of ligand and complexes onto a sample holder and sputter-coated with a thin layer of conductive material, such as gold, to improve the conductivity and minimize charging effects during imaging. The SEM images of the ligand was uniform and well-defined particles with surface features, indicating its crystalline nature and regular

crystal growth as shown in Fig. 1. The morphology of the ligand appeared to be in the form of amorphous and microcrystalline structures, which showed a characteristic shape and size distribution.

While the SEM image of organotin(IV) complexes showed different particle size and surface texture, indicating the effect of the coordination of Schiff base ligand with organotin(IV) moieties as shown in Fig. 1. These changes in surface morphology may suggest the formation of larger aggregates or the presence of new surface features resulting from the coordinated bonds. In general, SEM analysis of the ligand and its complexes provide a valuable evidence about the surface characteristics and morphological features. This characterization technique added other analytical methods and contributed to a comprehensive understanding of the complexation of ligand and organotin(IV) complexes.



**Fig. 1** SEM images of **a** Ligand (L), **b**  $\text{Ph}_3\text{SnL}$  complex, **c**  $\text{Bu}_3\text{SnL}$  complex, and **d**  $\text{Me}_3\text{SnL}$  complex

### 2.8.2 Energy dispersive X-ray (EDX)

EDX was used to provide the elemental composition of the prepared complexes. EDX analysis allows the identification and quantification of elements exist in the ligand and synthesised complexes based on their characteristic X-ray emission spectra. A small amount of the samples were mounted on a sample holder, and the EDX detector was positioned to capture the X-ray emissions generated by the interaction of the sample with an electron beam. The detector measures the energy and intensity of the X-rays emitted by the elements present in the prepared samples [28].

EDX analysis of the ligand provided an information about the elements constituting the ligand molecule. The spectrum obtained revealed the presence of carbon, hydrogen, nitrogen, and oxygen, which are typically found in synthesized organic compound (L) as shown in Fig. 2. The relative intensities of the peaks in the spectrum provide insights into the stoichiometry of the synthesized ligand. In the case of the organotin(IV) complexes, EDX analysis confirm the presence of tin (Sn) along with the elements identified in the ligand spectrum as shown in Fig. 2. The relative intensities of the tin peaks compared to the ligand peaks indicated the successful coordination of the ligand with the tin atom in the complexes. The existence of additional elements in the EDX spectrum could provide information about other possible impurities or elements obtained during the synthesis.

### 2.8.3 Fourier transform infrared spectroscopy (FTIR)

FTIR was utilized to provide information about the functional groups exist in the prepared complexes by measuring the absorption of infrared by the molecules [29]. The specific band at  $3469\text{ cm}^{-1}$ , indicates the presence of O–H stretching, and the bands at  $3097\text{ cm}^{-1}$  and  $2926\text{ cm}^{-1}$  were assigned to aromatic C–H stretching, while the band at  $1636\text{ cm}^{-1}$  indicated the presence of C=O group. In addition, a band at  $1592\text{ cm}^{-1}$  assigned to the presence of C=N of Schiff bases.

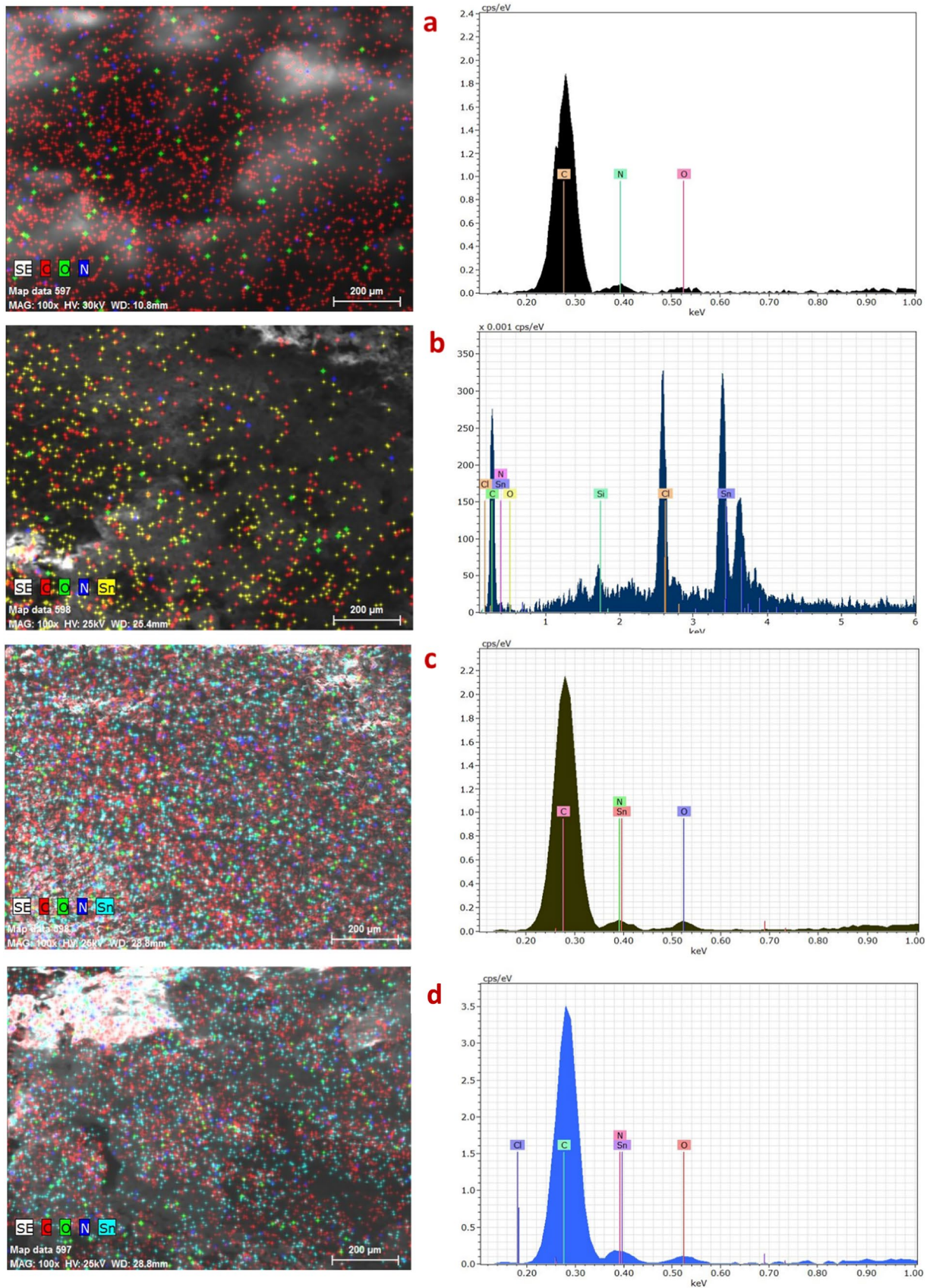
For the  $\text{Ph}_3\text{SnL}$  complex, the FTIR showed similar bands as the ligand, with a small shifts. The O–H stretching bands recognised at  $3469\text{ cm}^{-1}$ , while the C–H stretching aromatic was at  $3098\text{ cm}^{-1}$ . The C–H stretching aliphatic were observed at  $2922\text{ cm}^{-1}$ . The C=O band was at  $1640\text{ cm}^{-1}$ , and the C=N observed at  $1589\text{ cm}^{-1}$ . A new bands were appeared at  $527\text{ cm}^{-1}$  and  $453\text{ cm}^{-1}$ , confirming the presence of Sn–C and Sn–O bonds in the complex. The FTIR of  $\text{Bu}_3\text{SnL}$  complex showed bands attributed to the ligand's functional groups [30]. The O–H stretching band observed at  $3472\text{ cm}^{-1}$ , while the C–H stretching aromatic observed at  $3097\text{ cm}^{-1}$ . The aliphatic C–H stretching were appeared as a very sharp and strong bands at  $2956\text{ cm}^{-1}$  and  $2921\text{ cm}^{-1}$ . The C=O and C=N bands gave two bands at  $1637$

$\text{cm}^{-1}$  and  $1598\text{ cm}^{-1}$  respectively. The presence of Sn–C and Sn–O bonds were confirmed by specific bands at  $525\text{ cm}^{-1}$  and  $451\text{ cm}^{-1}$  respectively. The FTIR of  $\text{Me}_3\text{SnL}$  complex showed O–H stretching band at  $3380\text{ cm}^{-1}$ , while the aromatic C–H stretching gave band at  $3095\text{ cm}^{-1}$ . The aliphatic C–H stretching were appeared at  $2940\text{ cm}^{-1}$ . The C=O and C=N bands appeared at  $1638\text{ cm}^{-1}$  and  $1590\text{ cm}^{-1}$  respectively. While, bands at  $527\text{ cm}^{-1}$  and  $452\text{ cm}^{-1}$  confirmed the presence of Sn–C and Sn–O bonds in the formation of the complexes [31]. All FTIR data for synthesized ligand and corresponding complexes were summarized in Table 2.

### 2.8.4 Nuclear magnetic resonance ( $^1\text{H-NMR}$ )

The  $^1\text{H}$  NMR spectrum of the synthesized Schiff base ligand (L) provides detailed information about its structural features and chemical environments as shown in Fig. 3 [32].  $8.43$  (s, 1H, N=CH), this peak corresponds to the proton of the imine group (N=CH), indicating the formation of the Schiff base. The singlet (s) nature of the peak suggests that this proton is not coupled to any nearby protons.  $8.02$  (s, 1H, OH) and  $7.82$  (s, 1H, OH), these peaks correspond to the hydroxyl (OH) protons, indicating the presence of two hydroxyl groups in the Schiff base. The singlet nature of these peaks suggests that these protons are not coupled to any nearby protons.  $7.33$  (d,  $J=8.5\text{ Hz}$ , 2H, Ar) and  $6.63$  (d,  $J=8.5\text{ Hz}$ , 2H, Ar), these peaks represent the aromatic (Ar) protons. The presence of a doublet (d) indicates that each of these aromatic protons is coupled to two neighboring protons, resulting in a splitting pattern with a coupling constant of  $8.5\text{ Hz}$ . Thus  $6.53$  (m, 2H, Ar) peak corresponds to two aromatic protons that show a multiplet (m) pattern. The multiplet suggests the presence of different neighboring protons, resulting in multiple splitting patterns. While  $6.46$  (m, 1H, Ar) peak represents a single aromatic proton that exhibits a multiplet pattern, indicating the presence of various neighboring protons. The influence of aromatic substitution on the chemical shift in proton NMR can be explained by the concept of electronic effects. Electron-donating groups, such as hydroxy or amine groups, can donate electron density to the aromatic ring, which leads to shielding of nearby protons. As a result, these protons experience a lower effective magnetic field and appear at lower chemical shift values as shown in Fig. 3.

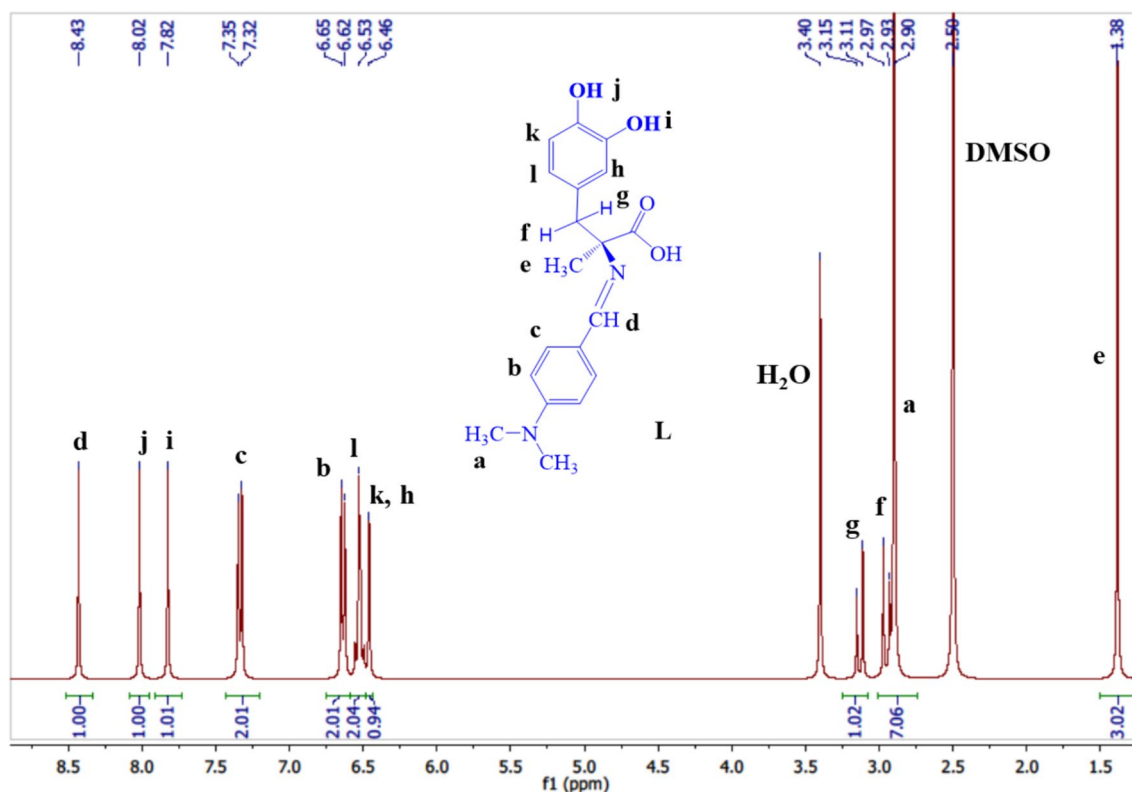
The peaks at  $3.13$  (d,  $J=12.4\text{ Hz}$ , 1H, CH) and  $2.95$  (d,  $J=12.4\text{ Hz}$ , 1H, CH) correspond to the methylene ( $\text{CH}_2$ ) protons adjacent to a chiral carbon atom. The presence of two doublet peaks arises due to diastereotopicity. In a chiral molecule, the two protons in the  $\text{CH}_2$  group experience different chemical environments, leading to non-equivalent coupling patterns. As a result, they give rise to two separate doublet peaks with a coupling constant of  $12.4\text{ Hz}$ .  $2.90$  (s, 6H,  $2\text{CH}_3$ ), this peak represents the methyl ( $\text{CH}_3$ ) groups,



**Fig. 2** EDX patterns of **a** Ligand (L), **b** Ph<sub>3</sub>SnL complex, **c** Bu<sub>3</sub>SnL complex and **d** Me<sub>3</sub>SnL complex

**Table 2** FTIR of ligand and complexes

Compounds	Wave number $\text{cm}^{-1}$						
	–OH	C–H Ar	C–H Alph	C=O	C=N	Sn–C	Sn–O
L	3469	3097	2926	1636	1592	–	–
$\text{Ph}_3\text{SnL}$	3469–3202	3098	2922	1640	1589	540	453
$\text{Bu}_3\text{SnL}$	3472–3199	3097	2956–2921	1637	1598	525	451
$\text{Me}_3\text{SnL}$	3380	3095	2940	1638	1590	527	452

**Fig. 3**  $^1\text{H}$ -NMR spectrum of ligand

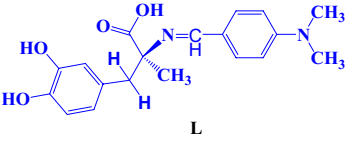
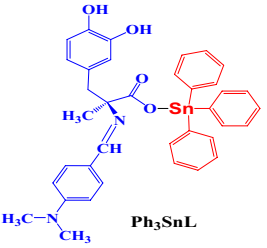
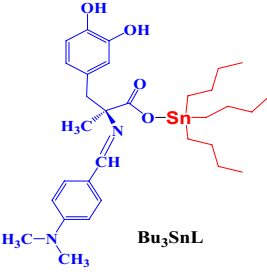
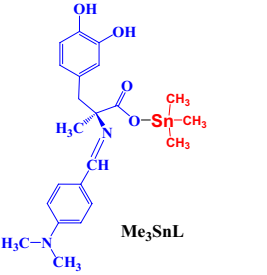
indicating the presence of two methyl groups in the Schiff base. The singlet nature of this peak suggests that these protons are not coupled to any neighboring protons. Finally the peak at 1.38 (s, 3H,  $\text{CH}_3$ ) chemical shift corresponds to the methyl ( $\text{CH}_3$ ) group, indicating the presence of a single methyl group. Similar to the previous case, the singlet nature of this peak suggests that these protons are not coupled to any neighboring protons.

The  $^1\text{H}$  NMR analysis of the synthesized Schiff base ligand (L) confirm the presence of different functional groups. The observations of singlets, doublets, multiplets, and diastereotopic splitting patterns support in the identification of specific proton and the characterization of the ligand's structural features. Table 3 summarized the  $^1\text{H}$  NMR spectrums data for the synthesized ligand and its complexes.

The  $^1\text{H}$  NMR spectrum of the synthesized  $\text{Ph}_3\text{SnL}$  complex provides insights into the changes in chemical shifts

compared to the ligand (L) alone. Let's discuss the spectrum in more detail and compare it to the ligand data see Table 3 and Fig. 4. The peak at 8.76 (s, 1H,  $\text{N}=\text{CH}$ ) corresponds to the proton of the imine group ( $\text{N}=\text{CH}$ ) in the complex. The chemical shift is slightly upfield compared to the ligand, indicating a change in the electronic environment due to coordination with the tin atom. Furthermore, the peak at 8.58 (s, 1H, OH) which assigned to the hydroxyl (OH) proton in the synthesized complex. Similarly, the imine group, the chemical shift is slightly upfield compared to the ligand, proposing the effect of the Sn coordination on the electronic field of the OH group. While, the peaks at 7.52–7.30 (m, 1H, OH; 2H, Ar; 15H, 3Ph groups), were assigned to the aromatic protons in the prepared complex. The multiplet (m) pattern indicates the existence of different neighboring protons. The chemical shifts of the aromatic protons show slight variations compared to the ligand, which demonstrate

**Table 3**  $^1\text{H-NMR}$  spectral data for ligand and metal complexes

Compound	$^1\text{H-NMR}$ (400 MHz: $\text{DMSO-d}_6$ , $\delta$ , ppm, $J$ in Hz)
 L	8.43 (s, 1H, N=CH), 8.02 (s, 1H, OH), 7.82 (s, 1H, OH), 7.33 (d, $J = 8.5$ Hz, 2H, Ar), 6.63 (d, $J = 8.5$ Hz, 2H, Ar), 6.53 (m, 2H, Ar), 6.46 (m, 1H, Ar), 3.13 (d, $J = 12.4$ Hz, 1H, CH), 2.95 (d, $J = 12.4$ Hz, 1H, CH), 2.90 (s, 6H, 2CH <sub>3</sub> ), 1.38 (s, 3H, CH <sub>3</sub> ).
 Ph <sub>3</sub> SnL	8.76 (s, 1H, N=CH), 8.58 (s, 1H, OH), 7.52-7.30 (m, 1H, OH, 2H, Ar, 15H, 3Ph groups), 6.75-6.58 (m, 5H, Ar, from L part), 3.28 (d, $J = 12.4$ Hz, 1H, CH), 3.01 (d, $J = 12.4$ Hz, 1H, CH), 2.90 (s, 6H, 2CH <sub>3</sub> ), 1.53 (s, 3H, CH <sub>3</sub> ).
 Bu <sub>3</sub> SnL	8.56 (s, 1H, N=CH), 8.17 (s, 1H, OH), 7.86 (s, 1H, OH), 7.33 (d, $J = 8.5$ Hz, 2H, Ar), 6.68-6.52 (m, 5H, Ar), 3.42 (d, $J = 12.4$ Hz, 1H, CH overlap with H <sub>2</sub> O peak), 2.99 (d, $J = 12.4$ Hz, 1H, CH), 2.88 (s, 6H, 2CH <sub>3</sub> ), 1.59 (s, 3H, CH <sub>3</sub> ), 1.45-1.25 (m, 12H, 6CH <sub>2</sub> ), 1.12-0.96 (m, 9H, 3CH <sub>2</sub> , 1CH <sub>3</sub> ), 0.66 (m, 6H, 2CH <sub>3</sub> ).
 Me <sub>3</sub> SnL	8.28 (s, 1H, N=CH), 8.03 (s, 1H, OH), 7.87 (s, 1H, OH), 7.28 (d, $J = 8$ Hz, 2H, Ar), 6.72-6.51 (m, 5H, Ar), 3.35 (d, $J = 16$ Hz, 1H, CH), 3.02 (d, $J = 16$ Hz, 1H, CH), 2.89 (s, 6H, 2CH <sub>3</sub> ), 1.46 (s, 3H, CH <sub>3</sub> ), 1.36 (s, 9H, 3CH <sub>3</sub> ).

an impact of Sn coordination on their electronic surroundings. The integration of this peak shows 18 hydrogen atoms 15 of them belongs to the three phenyl groups linked to the tin atom. 6.75–6.58 (m, 5H, Ar, from L part) peaks represent the aromatic protons originating from the ligand portion. The multiplet pattern predict the existence of different adjusting protons. Similarly, the aromatic protons in the prepared complex, the chemical shifts of these protons show slight differences compared to the ligand, which predict a limited impact of Sn coordination. Peaks at 3.28 (d,  $J = 12.4$  Hz, 1H, CH) and 3.01 (d,  $J = 12.4$  Hz, 1H, CH): were attributed to the methylene (CH<sub>2</sub>) protons next to the chiral carbon atom in the complex. The existence of doublets predict the coupling with one adjacent proton, and the chemical shifts are similar to those in the ligand, proposing that the Sn coordination has a minimal effect on these protons. The peak at 2.90 (s, 6H, 2CH<sub>3</sub>), attributed to the methyl (CH<sub>3</sub>) groups in the prepared complex. The chemical shift was similar compared to the ligand, demonstrating that the Sn coordination does

not affect the electronic surroundings of these groups. The peak at 1.53 (s, 3H, CH<sub>3</sub>), attributed to the methyl (CH<sub>3</sub>) group, and the chemical shift as same as the ligand, demonstrating that the Sn coordination has minimal impact on the electronic field of this group.

Generally, the  $^1\text{H NMR}$  of the synthesized Ph<sub>3</sub>SnL complex shows slight changes in chemical shifts compared to the ligand, which predicting some electronic changes according to the coordination with the Sn atom. On the other hand, the overall structural features and chemical structure of the ligand are conserved in the complex. The aromatic protons and the methylene protons adjacent to the chiral carbon show slight differences in their chemical shifts, which predict an impact of Sn coordination on their electronic surroundings. The -CH<sub>3</sub> groups show no changes, predicting that they are no influenced by Sn atom.

The  $^1\text{H NMR}$  analysis of the Bu<sub>3</sub>SnL complex gave information about the changes in chemical shifts related to the ligand (L) (Fig. 5). The peak at 8.56 (s, 1H, N=CH attributed

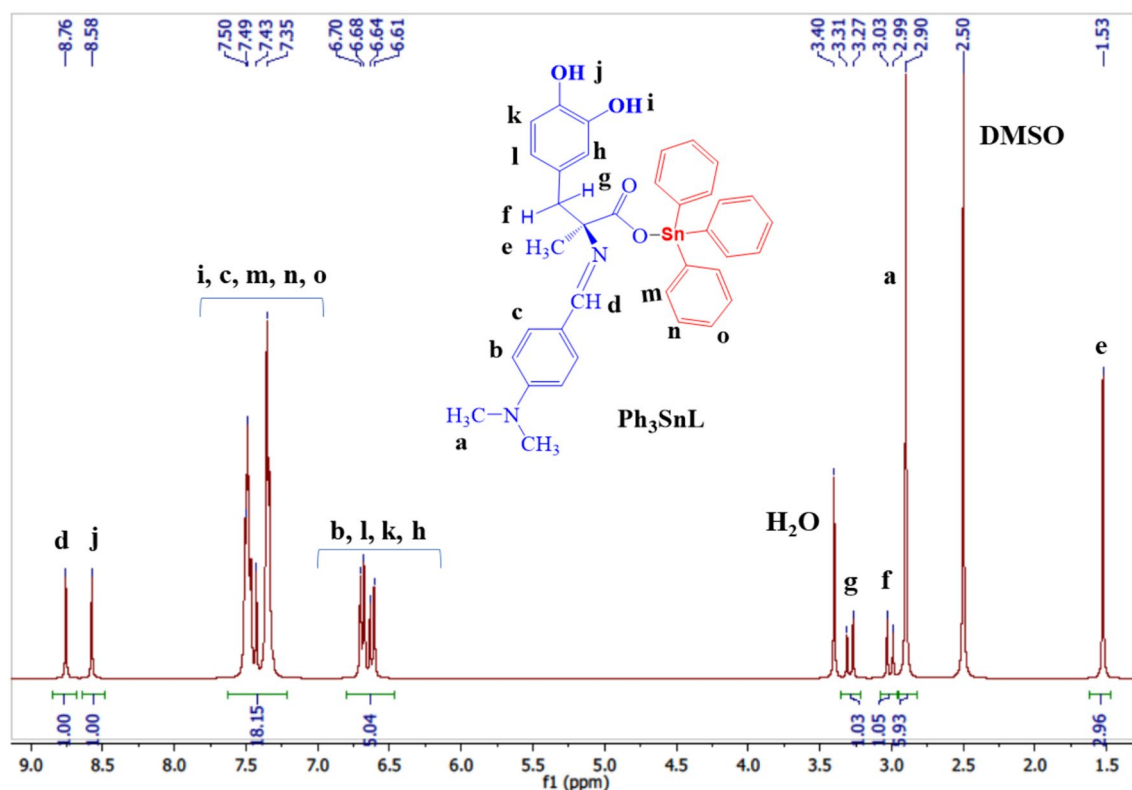


Fig. 4 <sup>1</sup>H-NMR spectrum of Ph<sub>3</sub>SnL complex

to the proton of the imine group (N=CH) in the prepared complex. The chemical shift is similar to the ligand, proposing that the electronic fields of this group is slightly affected by the coordination with the butyltin group. While the peak at 8.17 (s, 1H, OH) and 7.86 (s, 1H, OH) assigned to the hydroxyl (–OH) protons in the synthesized complex. The chemical shifts are quite similar to those in the ligand, predicting that the coordination with the butyltin group has negligible effect on the electronic fields of the –OH groups. The peak at 7.33 (d,  $J=8.5$  Hz, 2H, Ar) attributed to the aromatic protons in the prepared complex.

The existence of a doublet pattern propose coupling with two adjusting protons, and the chemical shift is similar to the ligand, predicting that the Sn coordination has a negligible impact on the electronic field of protons. The peak at 6.68–6.52 (m, 5H, Ar) attributed to the aromatic protons in the complex. The multiplet pattern proposed the presence of different neighboring protons. The chemical shifts are similar to those in the ligand, indicating that the tin coordination does not significantly affect the electronic environment of these protons. 3.42 (d,  $J=12.4$  Hz, 1H, CH): This peak corresponds to the methylene (CH<sub>2</sub>) proton adjacent to the chiral carbon atom in the complex. The presence of a doublet indicates coupling with one neighboring proton. The chemical shift is slightly upfield compared to the ligand,

indicating some electronic modifications upon coordination with the butyltin group. 2.99 (d,  $J=12.4$  Hz, 1H, CH): This peak represents another methylene (CH<sub>2</sub>) proton adjacent to the chiral carbon atom in the complex. The presence of a doublet indicates coupling with one neighboring proton. The chemical shift is comparable to the ligand, suggesting that the tin coordination has minimal influence on the electronic environment of this proton. 2.88 (s, 6H, 2CH<sub>3</sub>): This peak represents the methyl (CH<sub>3</sub>) groups in the complex. The chemical shift remains unchanged compared to the ligand, indicating that the tin coordination does not significantly affect the electronic environment of these groups. 1.59 (s, 3H, CH<sub>3</sub>): This peak corresponds to the methyl (CH<sub>3</sub>) group. The chemical shift remains the same as in the ligand, indicating that the tin coordination has minimal influence on the electronic environment of this group. <sup>1</sup>H NMR also showed 1.45–1.25 (m, 12H, 6CH<sub>2</sub>), 1.12–0.96 (m, 9H, 3CH<sub>2</sub>, 1CH<sub>3</sub>), and 0.66 (m, 6H, 2CH<sub>3</sub>) peaks represent the CH<sub>2</sub> and CH<sub>3</sub> groups of the three butyl groups linked to tin atom with integration all together 27 hydrogen atom which is exactly represents the butyl groups.

The <sup>1</sup>H NMR spectrum of the synthesized Bu<sub>3</sub>SnL complex shows minor changes in chemical shifts compared to the ligand, indicating some electronic modifications upon coordination with the butyltin group. However, the overall

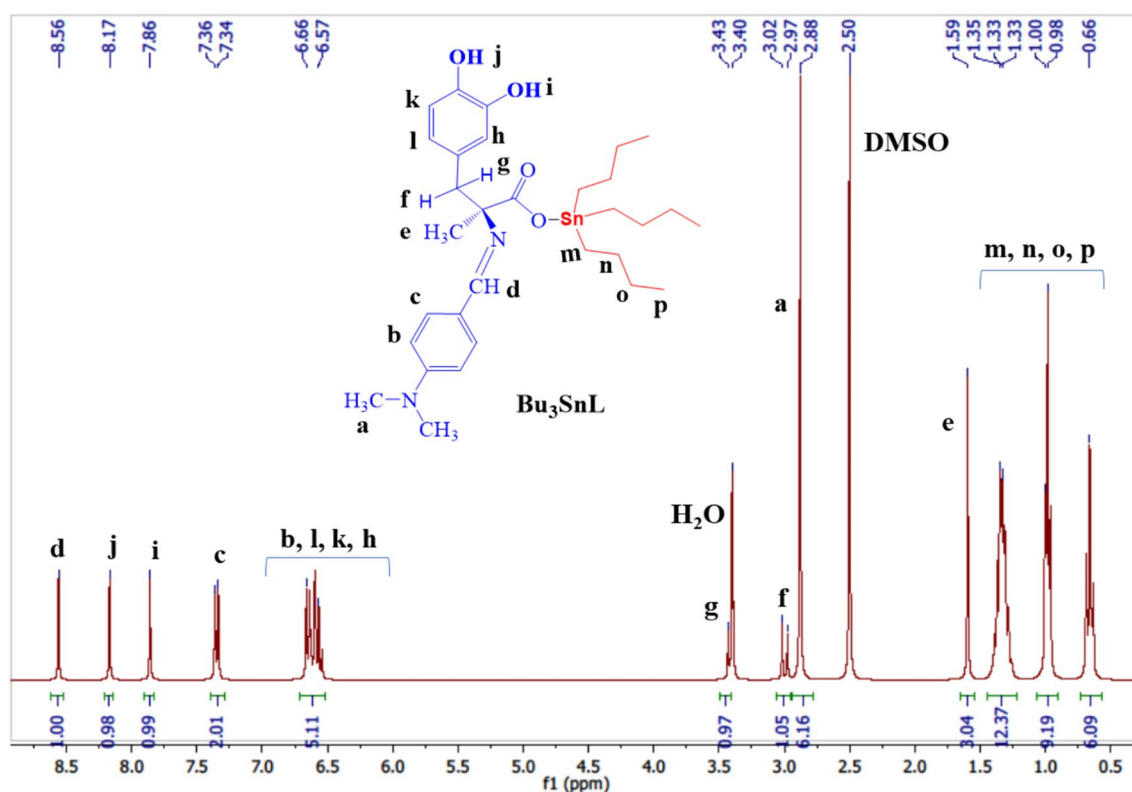


Fig. 5  $^1\text{H}$ -NMR spectrum of  $\text{Bu}_3\text{SnL}$  complex

structural features and chemical environments of the ligand are preserved in the complex. The imine group, hydroxyl groups, aromatic protons, and the methylene groups exhibit chemical shifts similar to those in the ligand, suggesting a limited influence of tin coordination on their electronic environments. But, the methylene proton adjacent to the chiral carbon atom shows a slightly upfield shift, indicating some electronic modifications due to the coordination with the butyltin group.

The  $^1\text{H}$  NMR analysis  $\text{Me}_3\text{SnL}$  complex gave changes in chemical shifts related to the ligand (L). The peak at 8.28 (s, 1H, N=CH) corresponds to the imine group (N=CH) proton in the complex. The chemical shift is somewhat downfield compared to the ligand, proposing an electronic change due to coordination with the methyltin group. While the peak at 8.03 (s, 1H, OH) and 7.87 (s, 1H, OH): attributed to the hydroxyl (OH) protons in the complex. The chemical shifts are similar to the ligand, predicting that the coordination with the methyltin group has negligible impact on the electronic field of the -OH groups. The peak at 7.28 (d,  $J=8$  Hz, 2H, Ar) corresponds to the aromatic protons in the prepared complex. The existence of a doublet indicates coupling with two adjoining protons, and the chemical shift is similar to the ligand, predicting that the Sn coordination does not effect on the electronic field of these protons. Moreover, the peak

at 6.72–6.51 (m, 5H, Ar) represent the aromatic protons in the complex. The multiplet pattern suggests the existence of different adjoining protons. The chemical shifts are similar to those in the ligand, indicating that the Sn coordination has slight effect on the electronic field of protons. Peaks at 3.35 (d,  $J=16$  Hz, 1H, CH) and 3.02 (d,  $J=16$  Hz, 1H, CH) assigned to the methylene ( $-\text{CH}_2$ ) protons in the complex. The presence of doublets confirms coupling with one adjoining proton, and the chemical shifts are equal to the ligand, proposing that the Sn coordination has a minimal effect on the electronic surroundings of these protons. Furthermore, the peaks at 2.89 (s, 6H,  $2\text{CH}_3$ ) represents the methyl ( $-\text{CH}_3$ ) groups next to N atom in the complex. The chemical shift remains the same as in the ligand, which indicate the Sn coordination does not influence the electronic environment of these groups. The peak at 1.46 (s, 3H,  $\text{CH}_3$ ) attributed to the methyl ( $-\text{CH}_3$ ) group. The chemical shift is similar to the ligand, which predict that the Sn coordination has a negligible impact on the electronic field of this group. Finally, the peak at 1.36 (s, 9H,  $3\text{CH}_3$ ): This peak represents the three methyl ( $\text{CH}_3$ ) groups in the complex connected to the Sn atom. In general, the  $^1\text{H}$  NMR analysis of the synthesized  $\text{Me}_3\text{SnL}$  complex demonstrate a slight changes in chemical shifts related to the ligand, indicating some electronic changes upon coordination with the methyltin group (Fig. 6).

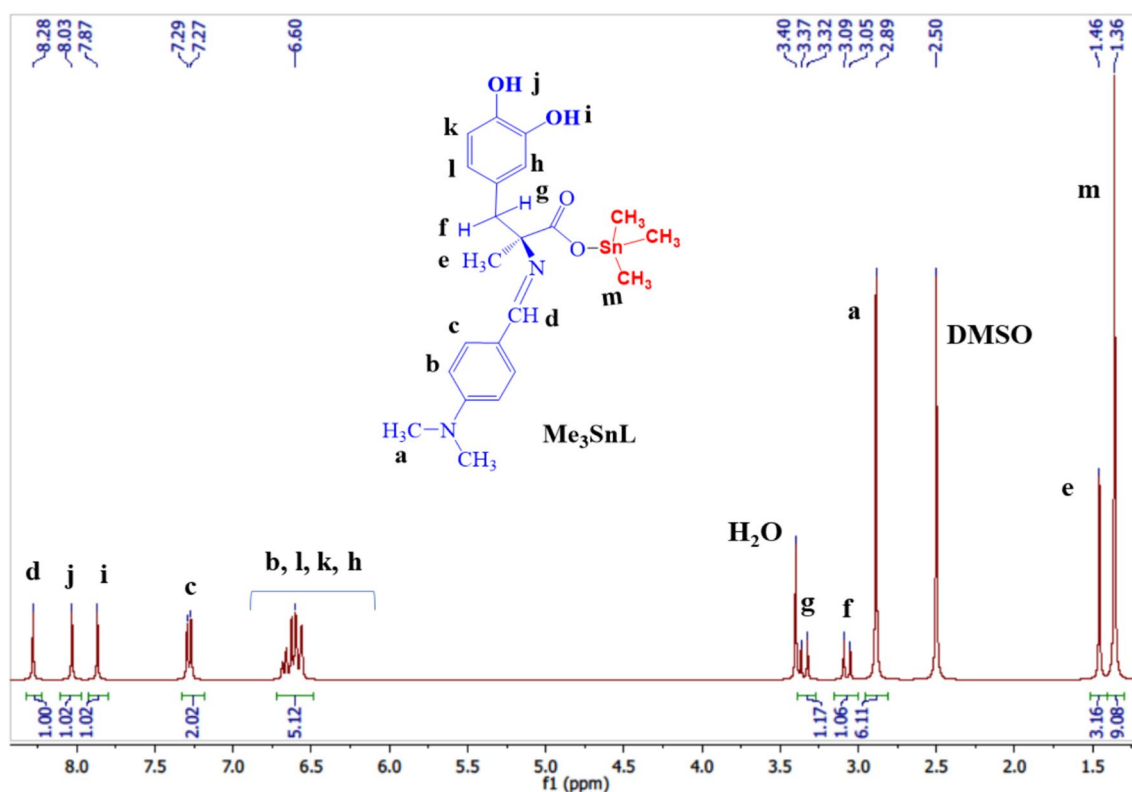


Fig. 6  $^1\text{H}$ -NMR spectrum of  $\text{Me}_3\text{SnL}$  complex

### 2.8.5 Nuclear magnetic resonance ( $^{13}\text{C}$ -NMR)

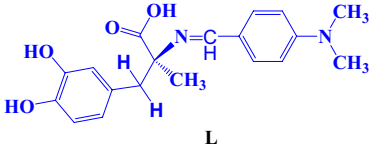
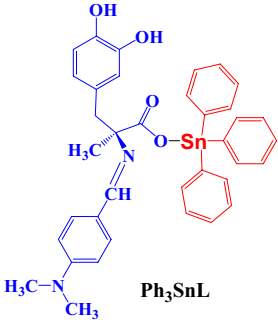
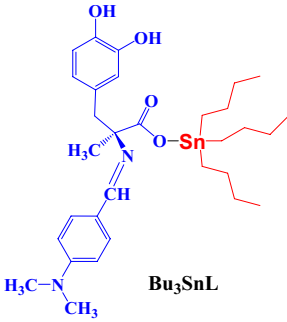
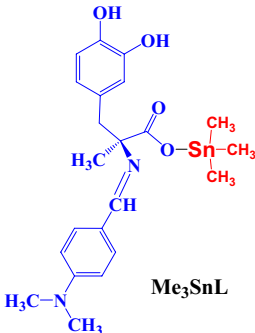
The synthesized ligand (L) and its tin complexes ( $\text{Ph}_3\text{SnL}$ ,  $\text{Bu}_3\text{SnL}$ , and  $\text{Me}_3\text{SnL}$ ) were characterized using  $^{13}\text{C}$  NMR spectroscopy to gain insight into their structural features and confirm the formation of the desired compounds. The  $^{13}\text{C}$  NMR spectra provide information about the carbon atoms present in the compounds and their chemical environments. Here is a brief discussion of the results [33, 34].

The  $^{13}\text{C}$  NMR spectrum of the ligand (L) would show signals corresponding to the carbon atoms in the methyl dopa and p-dimethylaminobenzaldehyde moieties. The chemical shifts in the ligand spectrum influenced by the substituents and structural arrangement (Table 4). The  $^{13}\text{C}$  NMR analysis of the Schiff base gave different peaks, demonstrating the presence of different types of carbon atoms within the ligand structure. The ligand gave peaks at 177.15 and 173.33 ppm, which can be assigned to carbon atoms in carbonyl ( $-\text{C}=\text{O}$ ) and azo-mthine groups ( $-\text{C}=\text{N}$ ). The chemical shifts predict the presence of electron-withdrawing groups or strong deshielding effects on these carbon atoms. A number of peaks in the range of (155.08 – 131.26) ppm indicate the presence of carbon atoms within the aromatic rings. The chemical shifts can vary depending on the substitution and adjusting functional groups. These carbon atoms

in the aromatic rings contribute to the overall aromaticity of the ligand and play a vital role in its chemical features. The chemical shifts at 59.27, 45.39, 41.90, and 21.24 ppm correspond to carbon atoms in aliphatic area, and these carbon atoms are a part of the ligand's backbone or side chains. The differences in the chemical shifts reveal to the differences in the local electronic fields and potential adjusting groups attached to these aliphatic carbon atoms. The detected chemical shifts provide understandings into the ligand's structure and chemical environment. The existence of carbonyl groups proposes the participation of the ligand in coordination chemistry. The aromatic rings is important in the ligand's stability and  $\pi$ -conjugation effects. On the other hand, the aliphatic areas provide information about the contribution to the ligand's solubility and reactivity. Through these results, we can confirm the formation of the compound and gain valuable information about its structural features. These understandings are vital for further studies and the succeeding formation of Sn complexes.

Two peaks observed at 177.15 and 173.33 ppm, which are attributed to carbonyl carbon atoms ( $-\text{C}=\text{O}$ ) and imine ( $-\text{C}=\text{N}$ ) groups of the Schiff base, these peaks undergo a significant downfield shift to 171.41 and 170.95 ppm, respectively in the prepared  $\text{Ph}_3\text{SnL}$  complex. This shift proposes a change in the electronic environment around

**Table 4**  $^{13}\text{C}$ -NMR spectral of ligand and metal complexes

Compound	$^{13}\text{C}$ -NMR (400 MHz: DMSO- $d_6$ , $\delta$ , ppm, $J$ in Hz)
 <p style="text-align: center;"><b>L</b></p>	177.15, 173.33, 155.08, 145.47, 144.30, 131.26, 127.04, 122.97, 121.71, 117.97, 117.65, 111.59, 59.27, 45.39, 41.90, 21.24.
 <p style="text-align: center;"><b>Ph<sub>3</sub>SnL</b></p>	171.41, 170.95, 155.08, 145.47, 144.30, 143.45, 134.37, 131.26, 131.03, 129.40, 127.04, 122.97, 121.71, 117.97, 117.65, 111.59, 58.72, 45.13, 41.90, 22.65.
 <p style="text-align: center;"><b>Bu<sub>3</sub>SnL</b></p>	171.41, 170.66, 155.08, 145.47, 144.30, 131.26, 127.04, 122.97, 121.71, 117.97, 117.65, 111.59, 58.72, 45.13, 41.90, 28.55, 24.29, 22.65, 14.01, 10.74.
 <p style="text-align: center;"><b>Me<sub>3</sub>SnL</b></p>	171.82, 171.41, 155.08, 145.47, 144.30, 131.26, 127.04, 122.97, 121.71, 117.97, 117.65, 111.59, 58.72, 45.13, 41.90, 22.65, 1.95.

the carbonyl groups upon coordination to the Sn atom. The peaks detected in the aromatic region of the spectrum (155.08, 145.47, 144.30, 143.45, 134.37, 131.26, 131.03, 129.40, 127.04, 122.97, 121.71, and 117.97 ppm) assigned to carbon atoms of the 's aromatic rings of ligand. These peaks come in accordance Ph<sub>3</sub>SnL with the ligand's data, indicating that the coordination of the Sn atom does not significantly change the electronic field of the aromatic rings. The presence of the Sn atom in the Ph<sub>3</sub>SnL complex is confirmed by the presence of a peak at 58.72 ppm, which attributed to the carbon atom bonded to Sn atom, and this peak does not appeared in the ligand's spectrum, which indicate

the characteristic feature of the Sn complex. While, the aliphatic group of the Ph<sub>3</sub>SnL (45.13, 41.90, and 22.65 ppm) shows peaks that come in accordance with the ligand's data. These peaks represent carbon atoms within aliphatic group of the ligand, prospective part of the ligand's backbone or side chains. Similarly, the chemical shifts suggests that coordination to the Sn atom does not influence the electronic environment of these carbon atoms.

The  $^{13}\text{C}$  NMR analysis of Bu<sub>3</sub>SnL provides valuable information about the structural features of the synthesized complex. Upon comparison with the ligand, the peaks in the Bu<sub>3</sub>SnL spectrum to the ligand's data, several changes

can be observed. These changes provide information of the effects of Sn atom on the ligand's electronic environment. The ligand shows peaks at 177.15 and 173.33 ppm, attributed to the carbonyl carbon atoms ( $-C=O$ ) and imine ( $-C=N$ ) groups in the Schiff base ligand. These peaks show downfield shifts to 171.41 and 170.66 ppm, respectively. This shift proposes a change in the electronic environment around the carbonyl groups upon coordination to the Sn atom. The aromatic area of the spectrum (155.08, 145.47, 144.30, 131.26, 127.04, 122.97, 121.71, and 117.97 ppm) shows peaks that come in accordance with the ligand's data. This indicates that coordination to the Sn atom does not have a significantly effect on the electronic environment of the ligand's aromatic rings. The presence of the Sn atom is confirmed by the existence of peak at 58.72 ppm, which assigned to the carbon atom bonded to the Sn atom. This peak is disappeared in the ligand's spectrum, indicating that it is a characteristic feature of the Sn complex. The aliphatic area of the  $Bu_3SnL$  spectrum (45.13, 41.90, 28.55, 24.29, 22.65, 14.01, and 10.74 ppm) also exhibits shifts a chemical shifts compared to the ligand's. These shifts propose changes in the electronic field of the ligand's aliphatic carbon atoms upon coordination with Sn atom. Remarkably, the presence of additional peaks in this region suggests the formation of butyl groups from the tributyltin moiety in the complex.

The  $^{13}C$  NMR analysis of  $Me_3SnL$  shoes Sn complex formation by Schiff base ligand with trimethyltin chloride ( $Me_3SnCl$ ), which provides a valuable knowledge of structural changes by Sn coordination. In comparison with the ligand's spectrum, we can investigate the effects of Sn coordination on the ligand's electronic environment. The  $^{13}C$  NMR show signals corresponding to the ligand carbon atoms, the methyl groups, and the Sn core center. The ligand carbon atoms might behave as a minor chemical shift changes due to coordination with Sn atom. Upon analysis the peaks in the  $Me_3SnL$  spectrum and compared to the ligand's data, we can observe several changes in chemical shifts, predicting the impact of Sn coordination on the ligand's structure. Generally, the ligand's spectrum, the presence of carbonyl carbon atoms ( $-C=O$ ) and Schiff base ( $-C=N$ ) groups in the Schiff base are confirmed by peaks at 177.15 and 173.33 ppm. Nevertheless, in the  $Me_3SnL$  spectrum, these peaks undergo remarkable higher chemical shifts to 171.82 and 171.41 ppm, respectively.

This suggests that tin coordination induces changes in the electronic environment around the aromatic carbon atoms next to high electronegative atoms such as oxygen and nitrogen. The aromatic region of the spectrum (155.08, 145.47, 144.30, 131.26, 127.04, 122.97, 121.71, and 117.97 ppm) exhibits peaks that align well with the ligand's data, suggesting that the coordination to the Sn atom does not significantly affect the ligand's aromatic rings. The presence of the tin atom in  $Me_3SnL$  is confirmed by the appearance of a peak

at 58.72 ppm, corresponding to the chiral carbon atom. In the aliphatic region of the  $Me_3SnL$  spectrum (45.13, 41.90, 22.65, and 1.95 ppm), we observe shifts in chemical shifts compared to the ligand's data. These shifts indicate changes in the electronic environment of the ligand's aliphatic carbon atoms due to tin coordination. The appearance of additional peaks in this region suggests the involvement of the methyl groups from the trimethyltin moiety in complex formation. The peak at 1.95 ppm, disappeared in the ligand's spectrum, confirming that it is a characteristic feature of the Sn complex. The  $^{13}C$  NMR spectrum of  $Me_3SnL$  demonstrates a significant changes in chemical shifts in comparable with the ligand's spectrum, specially for the carbonyl carbon atoms involved in Sn coordination, and the aliphatic carbon atoms affected by the presence of the methyl groups. On the other hand, the aromatic area shows good agreement between the complex and the ligand, indicating a negligible impact on the electronic environment of the ligand's aromatic rings. These results provide a valuable insights into the structural and electronic changes induced by tin coordination and contribute to the comprehensive characterization of the complex.

### 2.8.6 Nuclear magnetic resonance ( $^{119}Sn$ -NMR)

The  $^{119}Sn$  NMR analysis provides an essential information about the electronic properties and coordination of Sn complexes, these complexes are,  $Ph_3SnL$ ,  $Bu_3SnL$ , and  $Me_3SnL$ . In comparison the chemical shifts of the Sn atom in these three complexes, we can find the behaviour of the Sn coordinated-ligand and the impact of different organotin groups on the coordination. The  $^{119}Sn$  NMR spectra, showed a chemical shifts of the Sn atom in the complexes at  $-217.31$  ppm,  $-235.57$  ppm and  $-259.57$  ppm for  $Ph_3SnL$ ,  $Bu_3SnL$  and  $Me_3SnL$  respectively. These chemical shifts are downfield compared to the reference compound, which indicate the effect of the ligand coordination on the electronic surroundings around the Sn atom [35]. The detected downfield shifts in the  $^{119}Sn$  NMR spectra can be attributed to the electronic effects of the different organotin groups and ligand. The ligand, resulting from the Schiff base formation between methyl dopa and p-dimethylaminobenzaldehyde, which contains different functional groups that can contribute to the coordination chemistry with Sn atom. The electron-donating and electron-withdrawing behaviour of these groups can influence the electron density around the Sn center, resulting in changes in the  $^{119}Sn$  chemical shifts. By comparing the chemical shifts of the Sn atom in the prepared complexes, we can find the arrangement:  $Ph_3SnL$  ( $-217.31$  ppm) >  $Bu_3SnL$  ( $-235.57$  ppm) >  $Me_3SnL$  ( $-259.57$  ppm). This arrangement proposes that the electronic fields around the Sn atom becomes more shielded as we move from  $Ph_3SnL$  to  $Bu_3SnL$  and then to  $Me_3SnL$ . This

can be attributed to the changing in electronic properties and steric effects of the different organotin groups.

## 2.9 Anticancer drugs

### 2.9.1 Cytotoxic effect of organotin(IV) complexes on A549 human cell

MTT assay can be utilised to evaluate the cytotoxicity of the synthesized tri-organotin(IV) complexes on human lung cancer cells (A549). This assay is based on the ability of living cells to inhibit a yellow tetrazolium salt (MTT) to a purple formazan creation via the activity of mitochondrial dehydrogenases [15, 36]. The colorimetric change reveal the viability of the cells, with a reduction in color that indicating cell death due to apoptosis. In this study, the tri-organotin(IV) complexes and the standard drug doxorubicin were dissolved in acidic medium of isopropanol solvent and diluted with culture medium. Different concentrations (0, 8, 16, 32, 62.5, 125, 250, 500, and 1000  $\mu\text{g/mL}$ ) of the complexes and doxorubicin were added to the A549 cells and incubated for 48 h. Then, MTT solution was added and further incubated for 4 h in the dark. The absorbance of the producing formazan was measured at 570 nm.

The inhibition of the tri-organotin(IV) complexes was measured by determining the half maximal inhibitory concentration ( $\text{IC}_{50}$ ). The  $\text{IC}_{50}$  value represents the concentration of the compounds that inhibits 50% of cell proliferation compared to the normal cells [37]. This parameter gave a valuable information about the influence of the complexes as anti-cancer (Tables 5 and 6). The results can be used to assess the cytotoxicity of the tri-organotin(IV) complexes against human A549 cancer cells. A lower  $\text{IC}_{50}$  value indicates a higher strength of the complexes to inhibit cell proliferation. The comparison with doxorubicin, as a chemotherapeutic drug, permits for evaluating the relative efficacy of the synthesized complexes in comparison to the standard [38].

The  $\text{IC}_{50}$  values obtained for the combination of the synthesized Schiff base ligand with different tri-organotin(IV) complexes which found to be 16.84  $\mu\text{g/mL}$  for  $\text{Ph}_3\text{SnL}$ ,

980.1  $\mu\text{g/mL}$  for  $\text{Me}_3\text{SnL}$ , and 11.63  $\mu\text{g/mL}$  for  $\text{Bu}_3\text{SnL}$ . The  $\text{IC}_{50}$  value reflects the concentration of the compounds required to inhibit 50% of cell proliferation compared to untreated cells [39]. In this circumstance, a lower  $\text{IC}_{50}$  value of (16.84  $\mu\text{g/mL}$ ) indicates a higher effectiveness and stronger cytotoxic effect of the compounds on the A549 lung cancer cells. The results demonstrate that the combination of the Schiff base ligand with  $\text{Ph}_3\text{SnL}$  showed the most powerful cytotoxic effect. This suggests a synergistic interaction between the ligand and Sn atom, which enhance a cytotoxic against the A549 cancer cells [40]. On the other hand, the  $\text{Me}_3\text{SnL}$  showed a higher  $\text{IC}_{50}$  value of (980.1  $\mu\text{g/mL}$ ), indicating a less cytotoxic effect associated to the other compounds. This proposes that the communication between ligand and  $\text{Me}_3\text{SnCl}$  may have a weaker synergistic effect on the A549 cells. Similarly,  $\text{Bu}_3\text{SnL}$  exhibited a relatively low  $\text{IC}_{50}$  value of about (11.63  $\mu\text{g/mL}$ ), indicating a significant cytotoxic effect. This indicates that  $\text{Bu}_3\text{SnL}$  possesses a strong cytotoxic properties towards human A549 cancer cells and may give a promise anti-cancer agent. These results gives the ability of tri-organotin(IV) complexes, especially  $\text{Ph}_3\text{SnL}$  and  $\text{Bu}_3\text{SnL}$ , as anti-lung cancer. Further studies are needed to discover their mechanism of action inside the human body to evaluate their activity towards cancer cells, and assess their therapeutic clinically. Statistical analysis and  $\text{IC}_{50}$  values are shown in Table 7 and Fig. 7.

This indicates its strong potential as an effective anticancer agent.  $\text{Bu}_3\text{SnL}$  also showed significant cytotoxicity with an  $\text{IC}_{50}$  value of 11.63  $\mu\text{g/mL}$ , suggesting its potential as an alternative candidate for further development.  $\text{Bu}_3\text{SnL}$  also showed significant cytotoxicity with an  $\text{IC}_{50}$  value of 11.63  $\mu\text{g/mL}$ , suggesting its potential as an alternative candidate for further development.

## 3 Conclusions

In conclusion, tri-organotin(IV) complexes were synthesised by the reaction with Schiff base ligand which produce by the reaction of methyl dopa with p-dimethyaminobenzaldehyde.

**Table 5** Effect of complexes and doxorubicin on A549 cells viability

Conc	SB + Ph3SnL		SB + Me3SnL		SB + Bu3SnL	
	Mean	SD	Mean	SD	Mean	SD
1,000	11.79	0.53	49.87	3.50	11.87	0.29
500	13.06	0.59	77.11	3.94	12.55	0.64
250	15.69	2.67	80.59	8.41	14.59	0.29
125	17.73	4.23	90.11	5.07	15.35	1.28
62.5	20.36	5.33	96.51	1.93	17.81	0.44
32	34.27	5.24	96.51	1.93	24.94	5.51
16	59.54	5.95	97.16	1.35	50.98	7.47
8	82.36	11.20	94.29	1.07	86.51	10.11

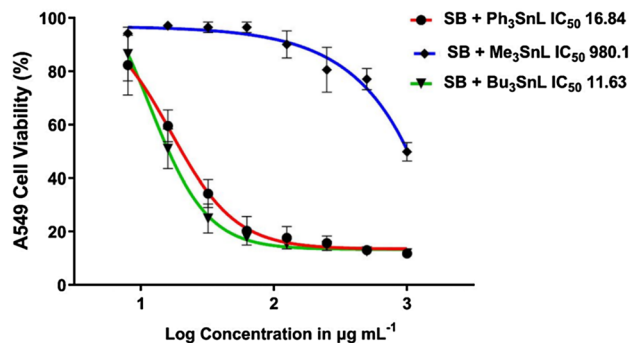
**Table 6** Tukey's multiple comparisons test

Tukey's multiple comparisons test	Below threshold	Summary	Adjusted <i>P</i> value
16			
SB + Ph <sub>3</sub> SnL vs. SB + Me <sub>3</sub> SnL	Yes	**	< 0.0001
SB + Ph <sub>3</sub> SnL vs. SB + Bu <sub>3</sub> SnL	Yes	*	0.0327
SB + Me <sub>3</sub> SnL vs. SB + Bu <sub>3</sub> SnL	Yes	**	< 0.0001
32			
SB + Ph <sub>3</sub> SnL vs. SB + Me <sub>3</sub> SnL	Yes	**	< 0.0001
SB + Ph <sub>3</sub> SnL vs. SB + Bu <sub>3</sub> SnL	Yes	*	0.0184
SB + Me <sub>3</sub> SnL vs. SB + Bu <sub>3</sub> SnL	Yes	**	< 0.0001
62.5			
SB + Ph <sub>3</sub> SnL vs. SB + Me <sub>3</sub> SnL	Yes	**	< 0.0001
SB + Ph <sub>3</sub> SnL vs. SB + Bu <sub>3</sub> SnL	No	ns	0.7199
SB + Me <sub>3</sub> SnL vs. SB + Bu <sub>3</sub> SnL	Yes	**	< 0.0001
125			
SB + Ph <sub>3</sub> SnL vs. SB + Me <sub>3</sub> SnL	Yes	**	< 0.0001
SB + Ph <sub>3</sub> SnL vs. SB + Bu <sub>3</sub> SnL	No	ns	0.7508
SB + Me <sub>3</sub> SnL vs. SB + Bu <sub>3</sub> SnL	Yes	**	< 0.0001
250			
SB + Ph <sub>3</sub> SnL vs. SB + Me <sub>3</sub> SnL	Yes	**	< 0.0001
SB + Ph <sub>3</sub> SnL vs. SB + Bu <sub>3</sub> SnL	No	ns	0.9397
SB + Me <sub>3</sub> SnL vs. SB + Bu <sub>3</sub> SnL	Yes	**	< 0.0001
500			
SB + Ph <sub>3</sub> SnL vs. SB + Me <sub>3</sub> SnL	Yes	**	< 0.0001
SB + Ph <sub>3</sub> SnL vs. SB + Bu <sub>3</sub> SnL	No	ns	0.9868
SB + Me <sub>3</sub> SnL vs. SB + Bu <sub>3</sub> SnL	Yes	**	< 0.0001
1000			
SB + Ph <sub>3</sub> SnL vs. SB + Me <sub>3</sub> SnL	Yes	**	< 0.0001
SB + Ph <sub>3</sub> SnL vs. SB + Bu <sub>3</sub> SnL	No	ns	0.9996
SB + Me <sub>3</sub> SnL vs. SB + Bu <sub>3</sub> SnL	Yes	**	< 0.0001

NS non-significant

\*\* *p* < 0.01\* *p* < 0.05**Table 7** Statistical analysis and IC<sub>50</sub> values of complexes and doxorubicin

Compound	IC <sub>50</sub> (μg mL <sup>-1</sup> )
SB + Ph <sub>3</sub> SnL	16.84
SB + Me <sub>3</sub> SnL	980.1
SB + Bu <sub>3</sub> SnL	11.63

**Fig. 7** Effect of complexes and doxorubicin in mean of A549 cells viability

The characterization of these complexes was acquired by diffenet analysis techniques, such as FTIR, SEM, <sup>1</sup>H NMR, <sup>13</sup>C NMR, and <sup>119</sup>Sn NMR. The resulted spectra gave a valuable information about the structure and coordination of organotin(IV) complexes. The cytotoxicity was evaluated towards A549 human lung cancer cell which demonstrate its activity as anti-cancer agents. The MTT assay shown concentration-dependent growth inhibition of the cancer cells, with Ph<sub>3</sub>SnL exhibiting the maximum cytotoxic effect among other synthesized complexes, which confirm by lowest IC<sub>50</sub> value of about (16.84 μg/mL). Bu<sub>3</sub>SnL shown a lower cytotoxicity with an IC<sub>50</sub> value of (11.63 μg/mL), while Me<sub>3</sub>SnL exhibited a relatively lower cytotoxic effect, with an IC<sub>50</sub> value of (980.1 μg/mL). The results highlighted the significance of the ligand structure and the behaviour of organotin(IV) complexes. The presence of different organotin(IV) groups have an effect towards anti-cancer agents. The observed cytotoxicity may be attributed to the ability of these complexes to impact with a vital cellular processes or to persuade apoptosis of cancer cells. Further investigations are necessary to demonstrate the mechanisms of action of these complexes, and their selectivity towards cancer cells, and their prospective for combination therapy.

**Acknowledgements** We thank Al-Nahrain University for technical support.

**Author contributions** F I, A A, A H and A Z A: experimental work, E Y, M B and N H: conceptualization, M A, A H J, A Z A and H H: writing—original draft, F I, H H, A B, A H and EY: review and editing.

**Funding** No funding was received to assist with the preparation of this manuscript.

**Data availability** Data is available upon reasonable request from the corresponding author.

## Declarations

**Conflict of interest** The authors declare no conflict of interest.

**Open Access** This article is licensed under a Creative Commons Attribution 4.0 International License, which permits use, sharing, adaptation, distribution and reproduction in any medium or format, as long as you give appropriate credit to the original author(s) and the source, provide a link to the Creative Commons licence, and indicate if changes were made. The images or other third party material in this article are included in the article's Creative Commons licence, unless indicated otherwise in a credit line to the material. If material is not included in the article's Creative Commons licence and your intended use is not permitted by statutory regulation or exceeds the permitted use, you will need to obtain permission directly from the copyright holder. To view a copy of this licence, visit <http://creativecommons.org/licenses/by/4.0/>.

## References

- Seebacher NA, Stacy AE, Porter GM, Merlot AM (2019) Clinical development of targeted and immune based anti-cancer therapies. *J Exp Clin Cancer Res* 38(1):156
- Al Talebi Z, Farhood AS, Hadi AG (2023) A comprehensive review of organotin complexes: synthesis and diverse applications. *Cancer Cell* 8:20
- Kumar M, Abbas Z, Tuli HS, Rani A (2020) Organotin complexes with promising therapeutic potential. *Curr Pharmacol Rep* 6:167–181
- Graisa AM, Zainulabdeen K, Salman I, Al-Ani A, Mohammed R, Hairunisa N, Mohammed S, Yousif E (2022) Toxicity and anti-tumour activity of organotin (IV) compounds. *Baghdad J Biochem Appl Biol Sci* 3(02):99–108
- Hadi AG, Jawad K, Ahmed DS, Yousif E (2019) Synthesis and biological activities of organotin (IV) carboxylates: a review. *Syst Rev Pharm* 10(1):26–31
- Hammoda RG, Shaalan N, Al-Mashhadani MH, Ahmed A, Yusop RM, Bufaroosha M, Yousif E (2023) Design, and synthesis of a plasticizer-Schiff's bases complexes as additive for polystyrene. *J Polym Res* 30(7):265
- Win YF, Yousif E, Ha ST, Majeed A (2013) Synthesis, characterization and preliminary in vitro antibacterial screening activity of metal complexes derivatives of 2-[[5-(4-Nitrophenyl)-1, 3, 4-thiadiazol-2-ylimino] methyl] phenol. *Asian J Chem* 25(8):4203
- Nordin ML, Abdul Kadir A, Zakaria ZA, Othman F, Abdullah R, Abdullah MN (2017) Cytotoxicity and apoptosis induction of *Ardisia crispa* and its solvent partitions against *Mus musculus* mammary carcinoma cell line (4T1). *J Evid Based Complement Altern Med* 16:2017
- Yaseen AA, Al-Tikrity ET, El-Hiti GA, Ahmed DS, Baashen MA, Al-Mashhadani MH, Yousif E (2021) A process for carbon dioxide capture using Schiff bases containing a trimethoprim unit. *Processes* 9(4):707
- Graisa AM, Husain AA, Al-Ani A, Ahmed DS, Al-Mashhadani MH, Yousif E (2022) The organotin spectroscopic studies of hydroxamic as a ligand: a systematic review. *Al-Nahrain J Sci* 25(1):14–23
- Jimaa RB, Al-Zinke JM (2021) A review on organotin (IV) thiosemicarbazone complexes, synthesis, characterization and biological activity. *J Anbar Pure sci* 15(2):66–73
- Gleeson B, Claffey J, Ertler D, Hogan M, Müller-Bunz H, Paradisi F, Wallis D, Tacke M (2008) el organotin antibacterial and anticancer drugs. *Polyhedron* 27(18):3619–3624
- Alkhamis K, Alatawi NM, Alsoliemy A, Qurban J, Alharbi A, Khalifa ME, Zaky R, El-Metwaly NM (2023) Synthesis and investigation of bivalent thiosemicarbazone complexes: conformational analysis, methyl green DNA binding and in-silico studies. *Arab J Sci Eng* 48:273–290
- Makia R, Al-Sammarae K, Al-Halbosiy M, Al-Mashhadani M (2022) In vitro cytotoxic activity of total flavonoid from *Equisetum Arvense* extract. *Rep Biochem Mol Biol* 11(3):487
- Ullah H, Previtali V, Mihigo HB, Twamley B, Rauf MK, Javed F, Waseem A, Baker RJ, Rozas I (2019) Structure-activity relationships of new organotin (IV) anticancer agents and their cytotoxicity profile on HL-60, MCF-7 and HeLa human cancer cell lines. *Eur J Med Chem* 181:111544
- Attanzio A, D'Agostino S, Busà R, Frazzitta A, Rubino S, Girasolo MA, Sabatino P, Tesoriere L (2020) Cytotoxic activity of organotin (IV) derivatives with triazolopyrimidine containing exocyclic oxygen atoms. *Molecules* 25(4):859
- Mogharbel AT, Hossan A, Abualnaja MM, Aljuhani E, Pashameah R, Alrefae SH, Abumelha HM, El-Metwaly NM (2023) Green synthesis and characterization of new carbathioamide complexes; cyclic voltammetry and DNA/methyl green assay supported by silico ways versus DNA-polymerase. *Arab J Chem* 16:104807
- Abbas Z, Kumar M, Tuli HS, Janahi EM, Haque S, Harakeh S, Dhama K, Aggarwal P, Varol M, Rani A, Sharma S (2022) Synthesis, structural investigations, and in vitro/in silico bioactivities of flavonoid substituted biguanide: a novel schiff base and its diorganotin (IV) complexes. *Molecules* 27(24):8874
- Wang J, Chen H, Song Q, Liu X, Li C, Wang H, Li C, Hong M (2022) Synthesis and *in vitro* cytotoxicity study of three diorganotin (IV) Schiff base di-acylhydrazone complexes. *J Inorg Biochem* 236:111983
- Banti CN, Hadjikakou SK, Sismanoglu T, Hadjiliadis N (2019) Anti-proliferative and antitumor activity of organotin (IV) compounds. An overview of the last decade and future perspectives. *J Inorg Biochem* 194:114–152
- Alqahtani AM, Abumelha HM, Alnoman RB, Abualnaja MM, Alsharief HH, Hameed A, Almontshery AM, El-Metwaly NM (2023) Copper (I)-catalysed synthesis of symmetrical perfluoroterphenyl analogues; fluorescence, antioxidant and molecular docking studies. *Luminescence* 38:1440–1448
- Ahmed AA, Al-mashhadani MH, Hashim H, Ahmed DS, Yousif E (2021) Morphological, color impact and spectroscopic studies of new schiff base derived from 1, 2, 4-triazole ring. *Prog Color Color Coat* 14(1):27–34
- Alhaydari E, Yousif E, Al-Mashhadani MH, Ahmed DS, Jawad AH, Bufaroosha M, Ahmed AA (2021) Sulfamethoxazole as a ligand to synthesize di- and tri-alkyltin (IV) complexes and using as excellent photo-stabilizers for PVC. *J Polym Res* 28(12):469
- Gorry M, Yoneyama T, Vujanovic L, Moss ML, Garlin MA, Miller MA, Herman J, Stabile LP, Vujanovic NL (2020) Development of flow cytometry assays for measuring cell-membrane enzyme activity on individual cells. *J Cancer* 11(3):702
- Jaafar ND, Al-Saffar AZ, Yousif EA (2020) Genotoxic and cytotoxic activities of lantadene A-loaded gold nanoparticles (LA-AuNPS) in MCF-7 cell line: an in vitro assessment. *Int J toxicol* 39(5):422–432
- Mahmood RI, Abbass AK, Al-Saffar AZ, Al-Obaidi JR (2021) An in vitro cytotoxicity of a novel pH-sensitive lectin loaded-cockle shell-derived calcium carbonate nanoparticles against MCF-7 breast tumour cell. *J Drug Delivery Sci Technol* 61:102230
- Awad AA, Hasson MM, faron Alfarhani B. (2019) Synthesis and characterization of a new Schiff base ligand type  $N_2O_2$  and their

- cobalt (II), nickel (II), copper (II), and zinc (II) complexes. *Int J Phys* 1294(5):52040
28. Mehmood N, Andreasson E, Kao-Walter S (2014) SEM observations of a metal foil laminated with a polymer film. *Procedia mater sci* 3:1435–1440
  29. Nikafshar S, Zabih O, Ahmadi M, Mirmohseni A, Taseidifar M, Naebe M (2017) The effects of UV light on the chemical and mechanical properties of a transparent epoxy-diamine system in the presence of an organic UV absorber. *Materials* 10(2):180
  30. Saleh TA, Al-Tikrity ET, Yousif E, Al-Mashhadani MH, Jawad AH (2022) Preparation of Schiff bases derived from chitosan and investigate their photostability and thermal stability. *Phys Chem Res* 10(4):549–557
  31. Ibrahim M, Nada A, Kamal DE (2005) Density functional theory and FTIR spectroscopic study of carboxyl group. *Indian J Pure Appl Phys* 43:911–917
  32. Mohammed A, Al-Mashhadani MH, Ahmed AU, Kassim MM, Haddad RA, Rashad AA, Al-Dahhan WH, Ahmed A, Salih N, Yousif E (2022) Evaluation the proficiency of irradiative poly (vinyl chloride) films in existence of di-and tri-organotin (IV) complexes. In *AIP Conference Proceedings* 2394(1).
  33. Tcharkhetian AE, Bruni AT, Rodrigues CH (2021) Combining experimental and theoretical approaches to study the structural and spectroscopic properties of flakka ( $\alpha$ -pyrrolidinopentiophenone). *Results Chem* 3:100254
  34. Pavia DL, Lampman GM, Kriz GS, Vyvyan JR. (2015) Introduction to spectroscopy.
  35. Hani R, Geanangel RA (1982)  $^{119}\text{Sn}$  NMR in coordination chemistry. *Coord Chem Rev* 44(2):229–246
  36. Shaheen F, Ali S, Shahzadi S (2017) Synthesis, characterization, and anticancer activity of organotin (IV) complexes with sodium 3-(1 H-Indol-3-yl) propanoate. *Russ J Gen Chem* 87:2937–2943
  37. Hadi NA, Mahmood RI, Al-Saffar AZ (2021) Evaluation of antioxidant enzyme activity in doxorubicin treated breast cancer patients in Iraq: a molecular and cytotoxic study. *Gene Rep* 24:101285
  38. Brauchle E, Thude S, Brucker SY, Schenke-Layland K (2014) Cell death stages in single apoptotic and necrotic cells monitored by Raman microspectroscopy. *Sci Rep* 4(1):4698
  39. Qiu YR, Zhang RF, Zhang SL, Cheng S, Li QL, Ma CL (2017) el organotin (IV) complexes derived from 4-fluorophenyl-selenoacetic acid: synthesis, characterization and in vitro cytostatic activity evaluation. *New J Chem* 41(13):5639–5650
  40. Guo JR, Chen QQ, Lam CW, Zhang W (2015) Effects of karanjin on cell cycle arrest and apoptosis in human A549, HepG2 and HL-60 cancer cells. *Biol Res* 48:1–7

**Publisher's Note** Springer Nature remains neutral with regard to jurisdictional claims in published maps and institutional affiliations.